PL-TR-97-2019 MFD-DTR-97-15695

Physical Mechanisms of Quarry Blast Sources

T. G. Barker
K. L. McLaughlin
J. Bonner

Maxwell Technologies - Federal Division
8888 Balboa Avenue
San Diego, CA 92123-1506

Scientific Report No. 1

January 1997

Approved for Public Release; Distribution Unilimited

DEPARTMENT OF ENERGY
Office of Nonproliferation and National Security
WASHINGTON, DC 20585

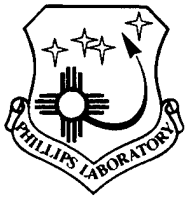

PHILLIPS LABORATORY
Directorate Of Geophysics
AIR FORCE MATERIEL COMMAND
HANSCOM AIR FORCE BASE, MA 01731-3010

SPONSORED BY
Department of Energy
Office of Non-Proliferation and National Security

"This technical report has been reviewed and is approved for publication."

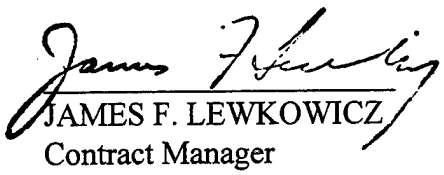

JAMES F. LEWKOWICZ
Contract Manager
Earth Sciences Division

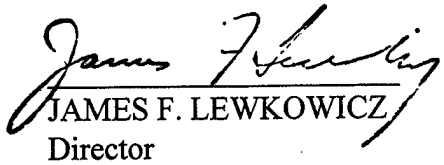

JAMES F. LEWKOWICZ
Director
Earth Sciences Division

Qualified requestors may obtain copies from the Defense Technical Information Center.

If your address has changed, or you wish to be removed from the mailing list, or if the addressee is no longer employed by your organization, please notify PL/IM, 29 Randolph Road, Hanscom AFB, MA 01731-3010. This will assist us in maintaining a current mailing list.

Do not return copies of this report unless contractual obligations or notices on a specific document requires that it be returned.

REPORT DOCUMENTATION PAGE

Form Approved
OMB No. 0704-0188

1. AGENCY USE ONLY *(Leave blank)*	2. REPORT DATE	3. REPORT TYPE AND DATES COVERED
	January 1997	Scientific Report No. 1

4. TITLE AND SUBTITLE

Physical Mechanisms of Quarry Blast Sources

5. FUNDING NUMBERS

Contract No.
F19628-95-C-0112
PE 69120H
PR DENN TR GM
WU AV

6. AUTHOR(S)

T. G. Barker, K. L. McLaughlin and J. Bonner

7. PERFORMING ORGANIZATION NAME(S) AND ADDRESS(ES)

Maxwell Technologies - Federal Division
8888 Balboa Avenue
San Diego, CA 92121-1506

8. PERFORMING ORGANIZATION REPORT NUMBER

MFD-DTR-97-15695

9. SPONSORING/MONITORING AGENCY NAME(S) AND ADDRESS(ES)

Phillips Laboratory
29 Randolph Road
Hanscom Air Force Base, MA 01731-3010
Contract Manager: James Lewkowicz/GPE

10. SPONSORING/MONITORING AGENCY REPORT NUMBER

PL-TR-97-2019

11. SUPPLEMENTARY NOTES

This research was sponsored by the Department of Energy, Office of Non-Proliferation & National Security, Washington, DC 20585

12a. DISTRIBUTION/AVAILABILITY STATEMENT

Approved for public release; distribution unlimited.

12b. DISTRIBUTION CODE

13. ABSTRACT *(Maximum 200 words)*

Models of quarry blasts may serve to develop efficient and robust methods for discriminating quarry blasts from other sources. In this report, we present progress on modeling quarry blasts at the Chemline quarry in central Texas and the Black Thunder mine in the Powder River Basin of Wyoming.

We observe strong variations in near field ground motions at the Black Thunder mine. Using estimates of site response derived from signal coda , we find that the variations are partly due to local structure. However, variations between nearly co-located shots indicate changes are also due to source mechanism. The data set provided to us at this time does not include all the data taken for these shots and it is anticipated that source and propagation effects can be resolved with the full data set. (Abstract continued on pg ii.)

14. SUBJECT TERMS		15. NUMBER OF PAGES
Quarry Blast	Seismic	50
Comprehensive Test Ban Treaty	Discrimination	16. PRICE CODE

17. SECURITY CLASSIFICATION OF REPORT	18. SECURITY CLASSIFICATION OF THIS PAGE	19. SECURITY CLASSIFICATION OF ABSTRACT	20. LIMITATION OF ABSTRACT
Unclassified	Unclassified	Unclassified	SAR

CLASSIFIED BY:

DECLASSIFY ON:

13. ABSTRACT (Continued from pg i)

We have used three dimensional finite difference calculations to interpret near-regional data from the Chemline quarry (Bonner, *et al.*, 1996). The focus here was to examine azimuthal variations and spall and compare them with the effects of local quarry topography. The spall model is the simplest explanation for the Love to Rg ratios and the Love wave radiation pattern. The Rg radiation pattern suggests that a combination of the spall and topographic models may be needed.

Table of Contents

List of Illustrations

List of Tables

1. Physical Mechanisms of Quarry Blast Sources

1.1 Introduction

Models of quarry blasts may serve to develop efficient and robust methods for discriminating quarry blasts from other seismic sources. In this report, we present progress on modeling quarry blasts at the Chemline quarry in central Texas and the Black Thunder mine in the Powder River Basin of Wyoming. In previous work (Barker, *et al.*, 1993a,b; and McLaughlin, *et al.*, 1994) we proposed physical models for the quarry blast source which included the effects of the 3D topography of the quarry face and the mass movement of the rock (spall). The intent of this work is to examine available quarry blast data and test these mechanisms for seismic excitation.

We have used three-dimensional finite difference calculations and wavenumber integration synthetics to interpret near-regional data from the Chemline quarry (Bonner, *et al.*, 1996). The focus here was to examine azimuthal variations and compare them with the effects of local quarry topography (as predicted by the 3D calculations) and the spall of material from the quarry face.

We observe strong variations in near field ground motions at the Black Thunder mine. Using estimates of site response derived from signal coda , we find that the variations are partly due to local structure. However, variations between nearly co-located shots indicate changes are also due to source mechanism. The data set provided to us at this time does not include all the data taken for these shots and it is anticipated that source and propagation effects can be resolved with the full data set.

2. Seismic Source Mechanisms for Quarry Blasts Observed Rayleigh and Love Wave Radiation Patterns from a Texas Quarry

2.1 Abstract

A theoretical understanding of the mechanisms by which quarry blasts excite seismic waves is useful in understanding how quarry blast discriminants may be transported from one region to another. A recent experiment in Texas with well-placed broadband stations and a cooperative blasting engineer has shed light on some of the physical mechanisms of seismic excitation at short periods (0.1 to 3 Hz). Azimuthal radiation patterns of the 0.2 to 2 Hz Rayleigh and Love waves are diagnostic of two proposed mechanisms for non-isotropic radiation from quarry blasts. Observations show that the Love and Rayleigh wave radiation patterns depend upon the orientation of the quarry benches. Two possible mechanisms for non-isotropic radiation are 1) the lateral throw of spalled material, and 2) the presence of the topographic bench in the quarry.

The spall of material can be modeled by vertical and horizontal forces applied to the free surface with time functions proportional to the derivative of the momentum of the spalled material. We use wavenumber integration synthetics to model the explosion plus spall in terms of seismic moment tensor sources plus point forces. Preliminary modeling using wavenumber integration synthetics demonstrate that the magnitude of the SH (Love) compared to the SV (fundamental Rayleigh or Rg) in the short period band (0.5 to 2 Hz) may be explained by the spall mechanism. Nearly all of the available mass must participate in the spall with an average velocity of 2 to 5 m/s to provide sufficient impulse to generate the observed Love waves. Love wave radiation patterns from such a mechanism are also consistent with the spall mechanism. However, the Rg radiation patterns from an explosion plus spall appear to somewhat differ from the observed pattern.

We modeled the effects of the topographic bench by using 3D linear finite difference calculations to compute progressive elastic wavefields from explosion sources behind the quarry bench. These 3D calculations show SH radiation patterns consistent with observations while the SV radiation patterns are not consistent with observations. We also find that the radiation patterns from the explosion behind the bench can not be modeled by a modified moment tensor as hypothesized by Barker, *et al.* (1993b). The 3D effects of the bench are more complicated than representation by a moment tensor with a single reduced horizontal couple as suggested by Barker, *et al.* The 3D finite difference synthetics exhibit polarity reversals in the outgoing P-SV waves (P, S, and Rg) radiated behind the bench. These theoretical results are under investigation in hopes that a simple representation can be found for the effects of the 3D bench.

Both mechanisms may contribute to the non-isotropic radiation patterns but the spall mechanism is the simplest physical mechanism that explains the bulk of the observations. Adjustments to the time functions for the horizontal force, the vertical force, and the explosion source may further refine remaining differences between prediction and the observations.

2.2 Introduction

Identification of large industrial blasts is an important problem in seismology. Earthquake seismologists wish to identify and exclude blasts from their catalogs in order to properly document natural activity. Furthermore in a CTBT context, it is necessary to identify blasts that could be mistaken for (or hide) a clandestine underground nuclear explosion. Several empirical methods have been found to successfully discriminate large industrial blasts from earthquakes (Smith 1989; Hedlin, *et al.*, 1990; Su, *et al.*, 1991; Smith 1993; Gitterman and vanEck 1993). Most methods rely upon the effects of ripple fire upon the seismic spectra (Willis 1963; Smith 1989; Hedlin, *et al.*, 1990). Ripple firing imposes scalloping upon the spectra and gives the spectra corner frequencies lower than those of microearthquakes with the same magnitude. The spectra then appear to be deficient in high frequencies. However, seismic spectra from non-ripple fired quarry detonations are also observed to be deficient in high frequency energy compared to microearthquakes (Smith 1993). It has been suggested that spall mechanisms contribute to low frequency seismic energy and the general tendency for quarry blasts to appear deficient in high frequency energies (Barker, *et. al.*, 1993a). This hypothesis has not been rigorously tested and questions remain as to the physical mechanisms by which these blasts excite regional waves and whether discrimination procedures can be transported to regions without prior experience. Therefore, blasts offer an opportunity to study the physics of seismic wave excitation and propagation while furthering our theoretical understanding of seismic discrimination.

It has long been observed that groups of seismograms from a single quarry at a fixed receiving station will often exhibit similar waveforms. Most microearthquake network operators learn to spot particular industrial sources by location and waveform characteristics. In fact, it has been suggested that waveform correlation methods and pattern recognition algorithms can be used to routinely identify blasting operations at known industrial sites (Harris 1991). However, in time, seismograms are recorded from the same industrial operation that differ significantly in waveform characteristics and do not correlate well with previous events. These differences are often blamed on variations in blasting practices and location within the quarry. It is just these variations in waveform characteristics that shed light upon the mechanisms of seismic excitation by the blasting operations.

In order to use the information contained in the variability of waveforms from a quarry, an experiment must be able to separate the effects of ripple fire, location within the quarry, and orientation of the quarry face. A cooperative quarry operator and good azimuthal coverage are beneficial. Bonner and Goforth (1995) noticed that the character of seismograms from a central Texas quarry were correlated with the orientation of the active quarry face as the quarry operations migrated within the quarry. In a subsequent study with good azimuthal coverage of a few blasts, Bonner, *et al.* (1996) inferred Rg radiation patterns from phase matched filtered Rg. They found Rg was enhanced behind the bench and attenuated for paths crossing the quarry floor. Delitsyne, *et al.* (1996) studied intermediate period Love waves from quarry blasts in Siberia. They found that the polarity of Love waves on opposing quarry faces were reversed and that blasts in the floor of the quarry produced small Love waves compared to Rg. They concluded that the Love wave polarity reversals and amplitude dependence were consistent with a spall mechanism for the generation of Love waves from the quarry faces and opening of a vertical tension crack for blasts in the quarry floor as suggested by the master crack model of Konya and Walter (1990).

In this study we attempt to model the data of Bonner, *et al.* (1996) to infer physical mechanisms for excitation of short-period fundamental Rayleigh (Rg) and Love (SH) waves. The Love wave and Rayleigh waves have been extracted by phase-matched filtering of recordings made at 10 azimuths around a quarry in central Texas. Three blasts conducted behind two perpendicular quarry benches were recorded. Two mechanisms are explored for non-isotropic radiation as suggested by Barker, *et al.* (1993a) and Barker, *et al.* (1993b). These two mechanisms are the throw (or spall) of rock and the near-source scattering of waves for explosions behind quarry faces.

2.3 Description of Quarry Blasts

Three blasts were recorded from the Chemical Lime Quarry, "Chemlime," in Central Texas summarized in Table 1, illustrated in Figure 1, and previously described in Bonner, *et al.* (1996). Each shot consisted of between 28 and 42 shots of about 165 lb. each (W=76 Kg) of ANFO spaced approximately D = 4 to 5 meters apart and approximately B = 4 to 5 meters behind the quarry face. We refer to D as the inter-shot spacing and B as the burden. The shots were fired with nominal delays of 27 milliseconds in a single line from either northwest to southeast or from southwest to northeast. The total duration of the first two shots were approximately 1.1 second and about 0.7 second for the second smaller shot. The quarry face is about 10 meters high and the three shots were fired behind two different faces of the quarry (the southwest and the southeast) and the ripple firing was directed either to the southeast or northeast as indicated in Figure 1. This inter-shot spacing, D, and burden, B, are consistent with standard shooting practices that move between 1000 and 10,000 times more rock than ANFO by

weight, and use scaled burdens, $B' = B/W^{1/3}$, of between 0.5 to 2 $m/Kg^{1/3}$ (Langefors and Kihlstrom 1963) The total yields of the three blasts were 3.16, 2.97, and 2.21 metric tons of ANFO.

Table 1. Chemical Lime, "Chemlime", Blasts

Date	# Holes	Total ANFO (lb.)	Powder Factor	Rock Moved (tons)	Quarry Face	Ripple Direction
June 28, 1994	42	6964	0.32	21,157	SW Face	NW to SE
June 12, 1994	40	6540	0.3	21,246	SW Face	NW to SE
July 17, 1994	28	4856	0.32	14,872	SE Face	SW to NE

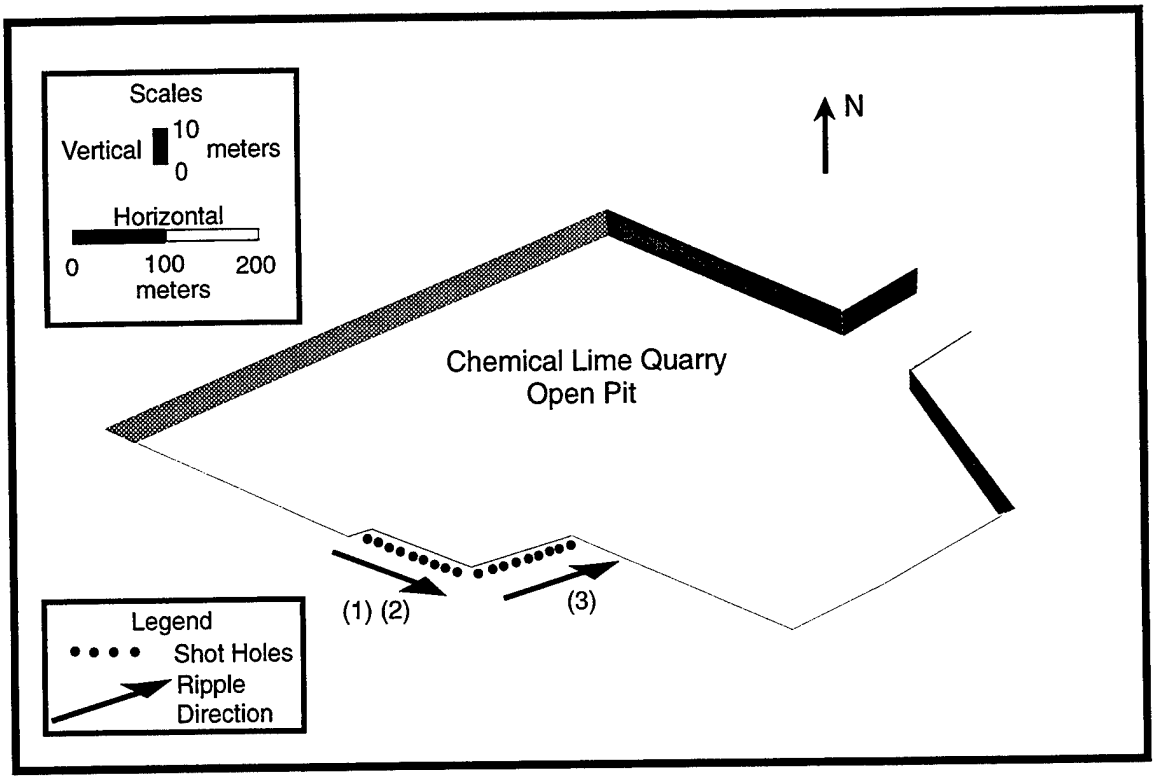

Figure 1. Diagram of the Chemlime quarry in central Texas. Shots 1 and 2 were blasted behind the southwest face and Shot 3 was blasted behind the southeast face. Ripple directions are indicated as northwest-to-southeast for shots 1 and 2 and southwest-to-northeast for shot 3. The quarry face is about 10 m high.

2.4 Seismic Velocity Models

The seismic recordings and Rayleigh wave matched filter processing are described in Bonner, *et al.* (1996). Between 6 and 7 stations recorded each shot on three component broadband sensors (Figure 2). Analysis of the Rg (short-period fundamental Rayleigh waves) resulted in a three layer model (Table 2). For the purposes of computation, this model was placed over a regional crustal model from Prewitt (1969). The 5 km of low velocity sediments are underlain by granites and other Greenvillian age rocks. Early calculations showed some anomalous phases resulting from the thick high Poisson's ratio layer with Vp = 5000 m/s and Vs = 1320 m/s. This layer was then replaced by a layer with linear gradients from the high Vp/Vs ratio of 2.6 at a depth of 1 km to a Vp/Vs ratio of about 1.67 at a depth of 5.2 km consistent with a decreasing Poisson's ratio with depth (see Tables 2 and 3). A fourth model is tabulated with discrete layers used for calculating wavenumber integration synthetics (Table 4).

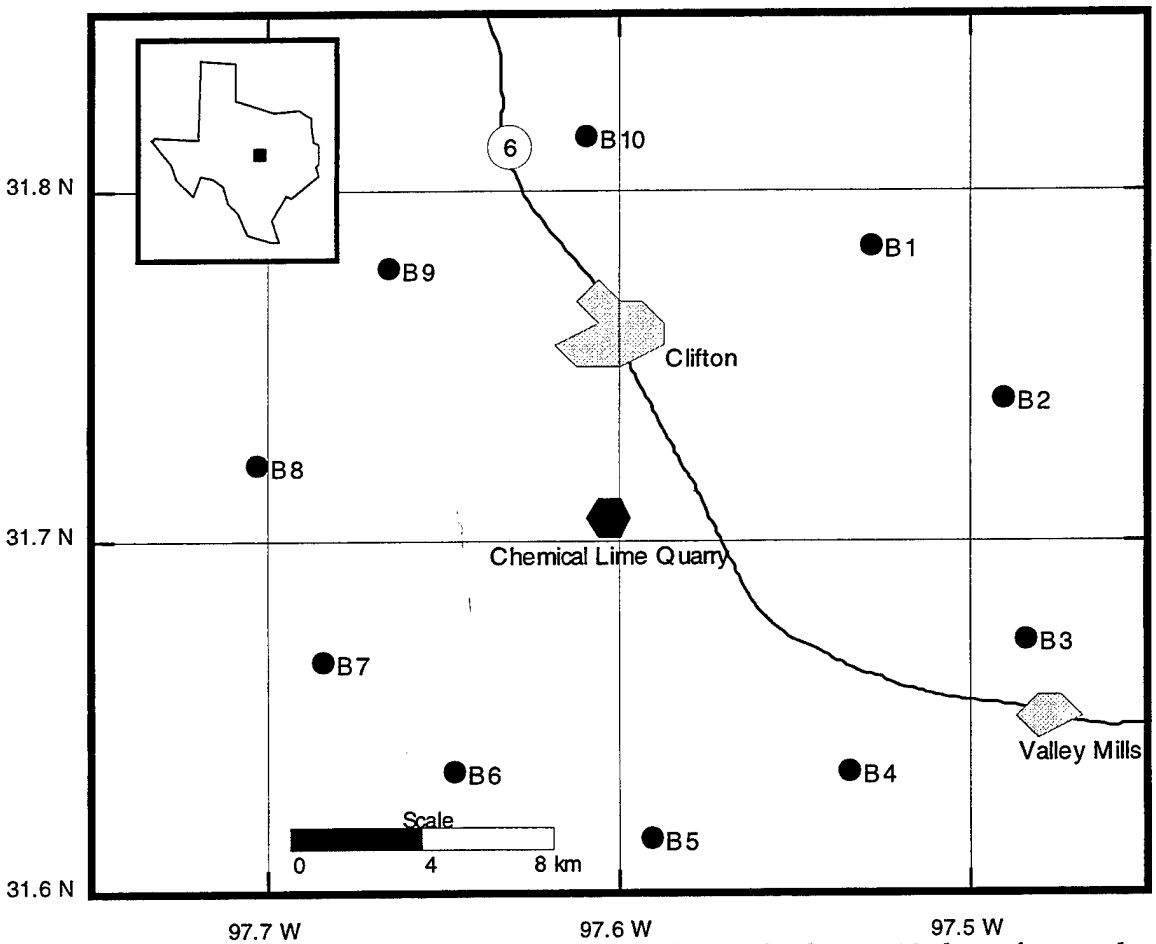

Figure 2. The 10 recording stations were located about 10 km from the Chemlime quarry.

Table 2. Original Velocity Model of Bonner, *et al.* (1996) on top of Prewitt (1969) Velocity Model

H (m)	Vp (m/s)	Vs (m/s)	Density (Kg/m^3)
300	3000	1000	1500
700	3100	1180	1600
4200	5000	1320	2500
14000	6140	Vp*.6	2500
11900	6720	Vp*.6	2500
8900	7100	Vp*.6	3000
half-space	8000	Vp*.6	3100

Table 3. Linear Gradient Velocity Model

H (m)	Vp (m/s)	Vs (m/s)	Density (Kg/m^3)
300	3000	1000	1500
700	3100	1180	1600
4200	linear gradient from 3468 to 5000	linear gradient from 1320 to 3000	2500
14000	6140	Vp*.6	2500
11900	6720	Vp*.6	2500
8900	7100	Vp*.6	3000
half-space	8000	Vp*.6	3100

Table 3a. Modified Linear Gradient Velocity Model

H (m)	Vp (m/s)	Vs (m/s)	Density (Kg/m^3)
300	2000	1000	1500
700	2100	1180	1600
4200	linear gradient from 2350 to 5000	linear gradient from 1320 to 3000	2500
14000	6140	Vp*.6	2500
11900	6720	Vp*.6	2500
8900	7100	Vp*.6	3000
half-space	8000	Vp*.6	3100

Table 4. Modified Velocity Model with Discrete Layers for Wavenumber Integration Synthetics

H (m)	Vp (m/s)	Vs (m/s)	Density (Kg/m^3)	Qμ
300	3000	1000	1500	50
700	3100	1180	1600	50
1200	3468	1320	2000	50
1000	3978	1880	2000	75
1000	4488	2440	2000	100
1000	5000	3000	2500	200
14000	6140	Vp*.6	2500	300
11900	6720	Vp*.6	2500	300
8900	7100	Vp*.6	3000	300
half-space	8000	Vp*.6	3100	500

2.5 Observed Radiation Patterns of Rayleigh and Love Waves

Figures 3-4 show the waveforms and inferred radiation patterns of short-period Rayleigh (Rg) and Love (SH) waves extracted from the seismograms of the three Chemlime shots. The radiation patterns show clear correlation with the orientations of the faces of the quarry. Love waves exhibit minima at azimuths perpendicular to the face of the quarry and maxima parallel to the quarry faces. Rayleigh waves (Rg) are enhanced behind the quarry face; to the southwest for shots 1 and 2 and to the southeast for shot 3. The correlation with the orientation with quarry face is clearly demonstrated by comparison of the patterns for shots 1 and 2 (oriented NW-SE) compared with shot 3 (oriented SW-NE). In addition, the radiation patterns show tendency for the amplitudes to be larger in the directions of the ripple fire; to the southeast for shots 1 and 2, and to the northeast for shot 3.

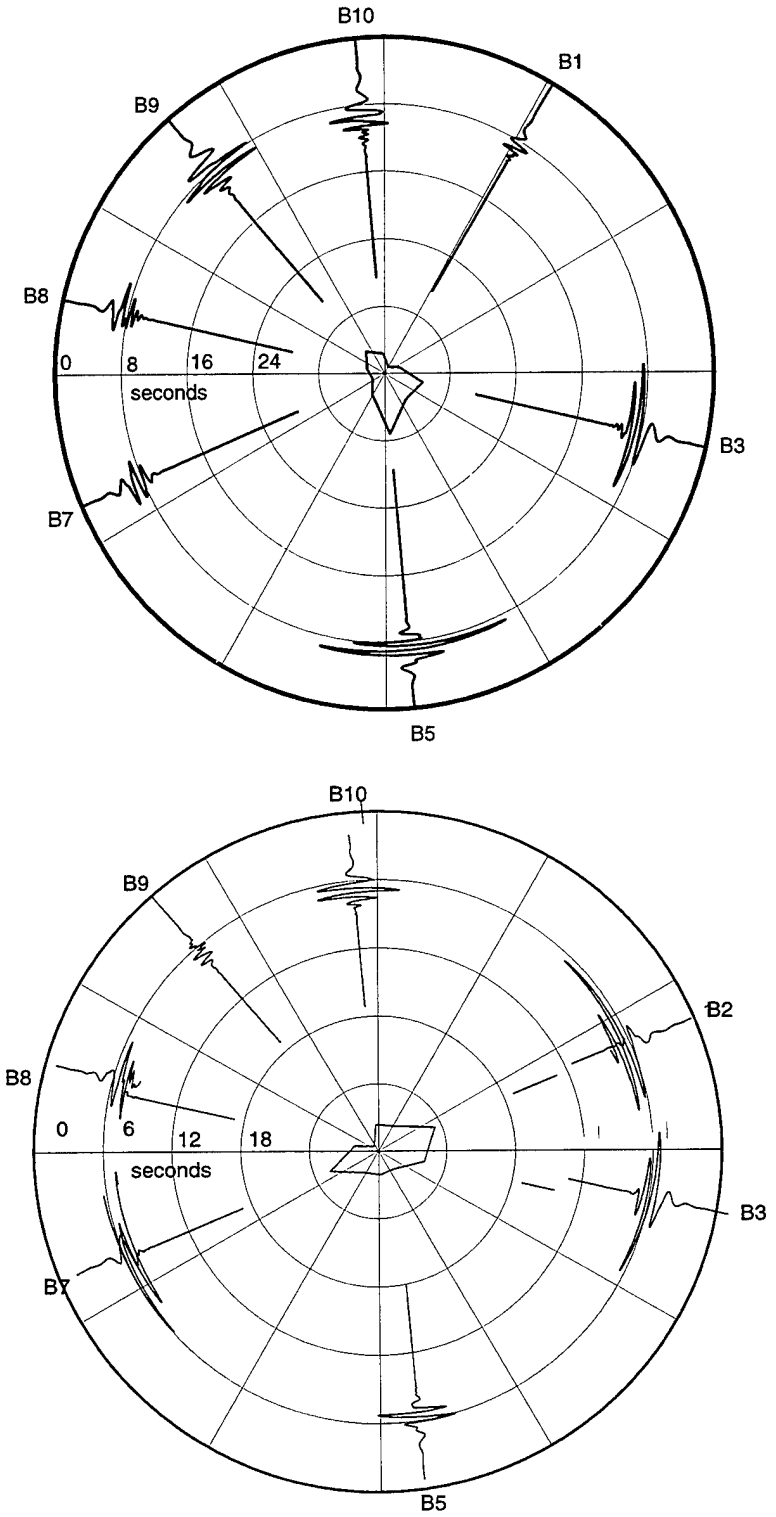

Figure 3. Love wave (SH) radiation patterns inferred for the June 28 (top) and July 17 (bottom) blasts located behind the southwest and southeast benches respectively.

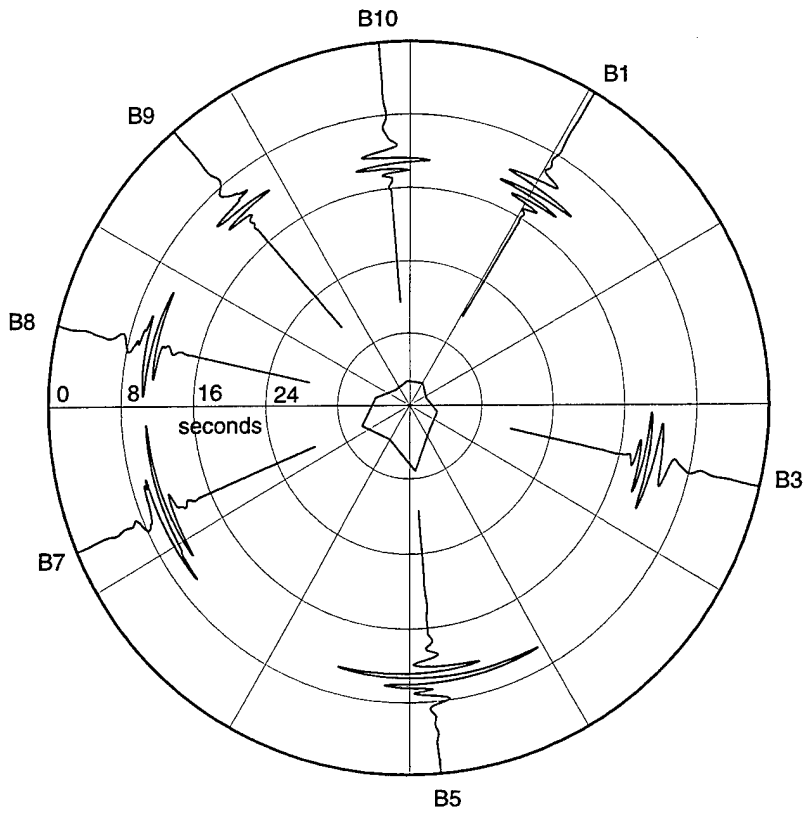

Figure 4. Rayleigh wave (Rg) radiation pattern inferred for the June 28 blast located behind the southwest bench and ripple fired from the northwest toward the southeast. Compare the Rg radiation pattern with the love wave radiation pattern at the top of Figure 3.

Figure 5 shows the ratios of Rg/SH amplitudes for shots 1 and 2 along the southwest bench. Rg/SH amplitudes are between 1 and 4 for stations 1, 2, 7, and 8 which are located to the northeast and southwest. Rg/SH amplitudes are less than 1 for stations 3, 5, 9, and 10 which are located to the southeast and northwest. Several stations were not operational during the 12 July (shot 2) event but the consistency of the Rg/SH ratios for the two shots along the same bench provides confidence that the Rg/SH patterns are reproducible for events on the same quarry face.

In the remainder of the report we examine two hypotheses to explain the enhancement of Rg behind the bench, Love wave radiation patterns, and the Love to Rg ratios. First, we examine the topographic bench using 3D finite differences. Second, we examine a spall model using plane-layered synthetics.

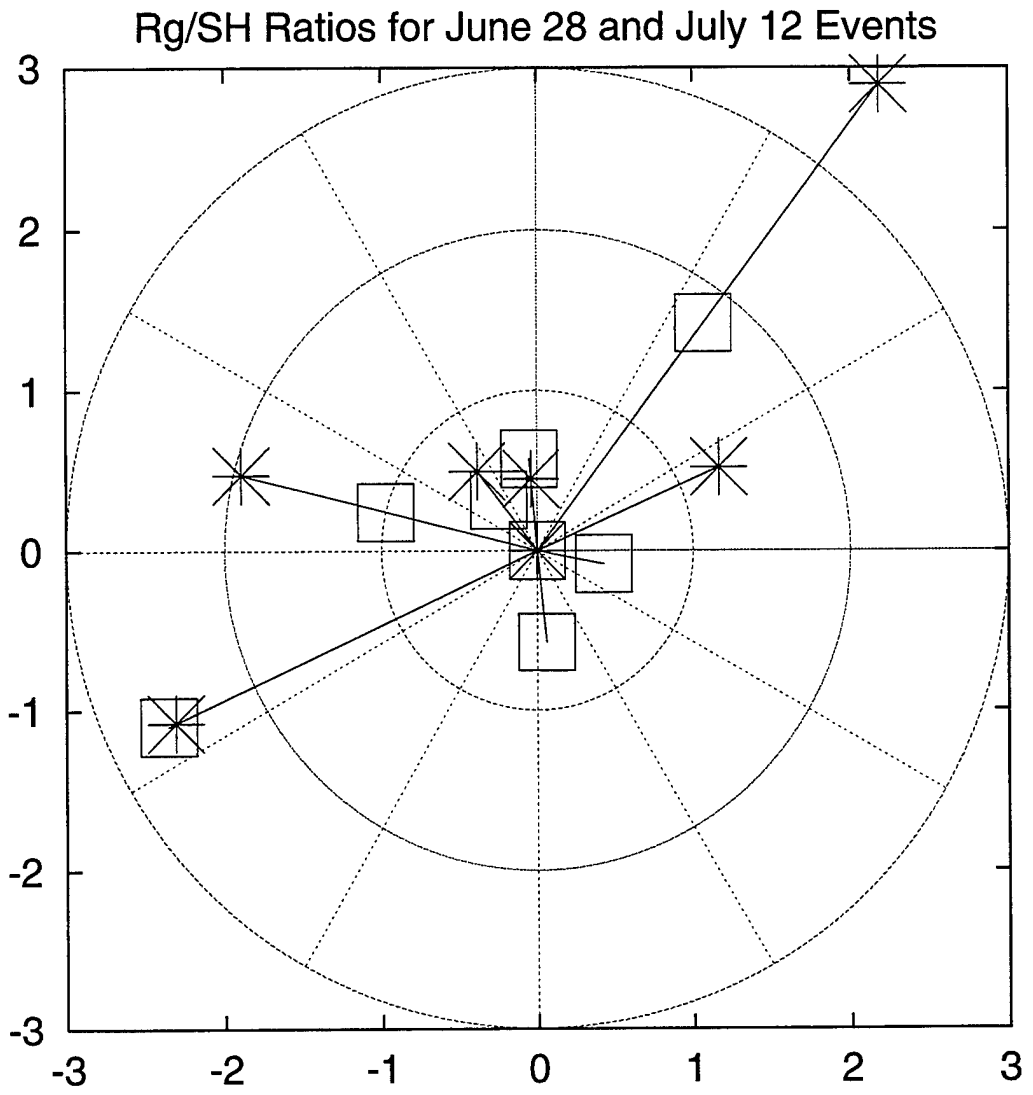

Figure 5. Amplitude Rg/SH ratios for blasts June 28 (squares) and July 12 (asterisks) Along the southwest quarry face. Stations 1, 2, 7 and 8 to the northeast and southwest (perpendicular to the quarry face) have Rg/SH ratios ≥ 1. While stations 3, 5, 9, and 10 to the southeast and northwest (parallel to the quarry face) have Rg/SH ratios < 1. The quarry face strikes northwest - southeast.

2.6 Finite Difference Calculations with Recursive Grid Refinement

We first wished to examine the near-source scattering problem of placing explosions behind a quarry bench. Barker, *et al.* (1993b) suggested the topographic bench introduces a radiation pattern to the far-field seismic waves. They further hypothesized that the radiation pattern could be modeled by an effective moment tensor source. The method of elastic finite differences with recursive grid refinement (see McLaughlin and Day, 1994) was used to model 3D wave propagation in this problem with a large range of

scales. The quarry was modeled with a fine grid of 5 m cells enclosed in a succession of coarser grids as illustrated in Figure 6. Eight levels of refinement were used with a refinement factor of 2 between successive levels. Each grid was composed of 63 wide by 63 long by 31 deep cells. The coarsest grid had a grid spacing of 640 m while the finest grid had a grid spacing of 5 m (see Table 5). This procedure allows us to model details of the quarry pit at a 5 m resolution in a small region and the wave propagation of 1 to 5 Hz waves to greater distance with coarse grids. Table 5 demonstrates the utility of the recursive grid refinement procedure. In order to grid the same volume that was gridded at the coarse 640 m spacing with a fine spacing of 5 m would have required $2.5*10^{11}$ cells instead of the $9.8*10^{5}$ cells which is both a great savings in memory as well as computation. However, since the fine grid does not extend outward from the quarry, each transition from fine grid to coarse grid results in trapping the high frequencies that do not propagate in the coarser grid. The resulting waves recorded in the coarser grids at greater and greater distance can only accurately support waves with frequencies lower than the Fmax listed in the Table 5. Therefore, some care must be taken to use only those portions of the synthetics that faithfully record the outgoing waves with appropriate bandwidth (lowpass filtered) before high frequency reflections arrive from either the bottom or outer boundaries of the coarser grids.

Table 5. Recursive Refinement Grid Tree

Level	dx,dy,dz (m)	dt (sec)	# cells	Grid Dimensions (m,m,m)	Vmax/Vmin (m/s)	Fmax (Hz)	grid-cycles (4 sec duration)
1	640	0.04	123039	39680,39680,19200	6140/3684	0.16	100
2	320	0.02	123039	19840,19840,9600	6140/3684	0.31	200
3	160	0.01	123039	9920,9920,4800	4824/2808	0.63	400
4	80	0.005	123039	4960,4960,2400	3964/1864	1.25	800
5	40	0.0025	123039	2480,2480,1200	3533/1392	2.5	1600
6	20	0.00125	123039	1240,1240,600	3100/1180	5.0	3200
7	10	0.000625	123039	620,620,300	3000/1000	10.	6400
8	5	0.0003125	123039	310,310,150	3000/1000	20.	12800
total			984312				25500

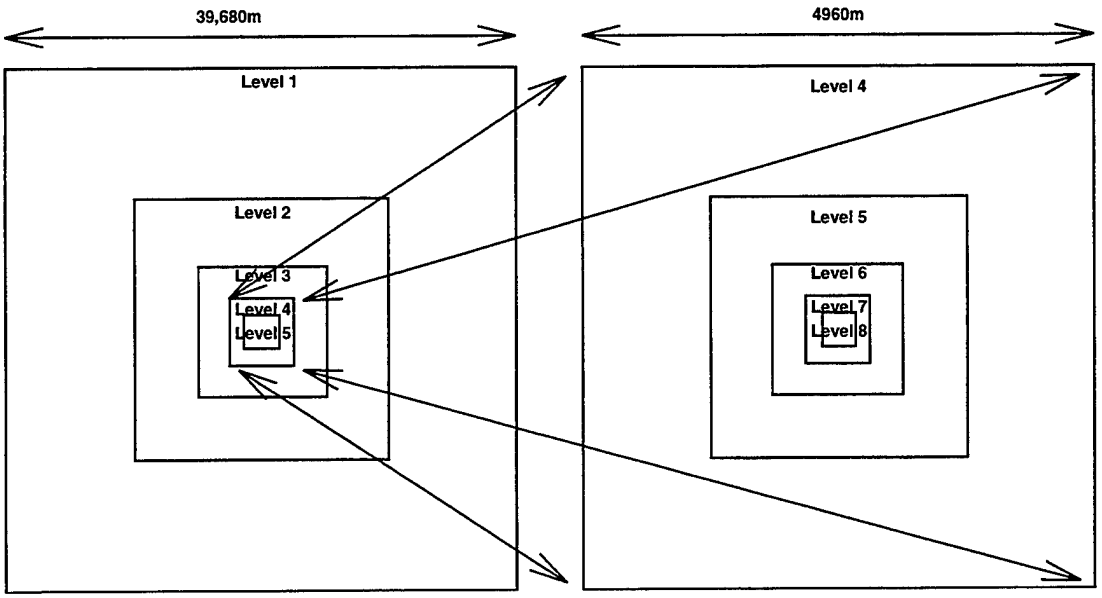

Figure 6. Diagram of recursive grid refinement used in finite difference calculations. Eight levels of refinement were used with one grid on each level resulting in an arrangement of nested grids. The quarry and explosion sources are located in the finest grid (level 8).

2.7 Numerical Calculation Series

Several numerical experiments were performed and are summarized in Table 6. First, an explosion source was placed in the upper 10 m of a laterally homogeneous layered half-space with no quarry present (shot _0). This "control" calculation could be compared with a wavenumber integration code for testing and validation. Next, the quarry pit was inserted into the finest grid (level 8 with 5 m resolution) by setting the elastic moduli of the appropriate cells to zero (shot_1). This implicitly forces the free surface boundary condition upon the topographic representation of the quarry pit. The explosion sources are inserted into the calculation by specifying the diagonal moment tensor components of appropriate cells with the relevant time delays. Each source was given a time function with a rise time of 0.25 seconds in order to remove spurious high frequencies from the calculation. This is equivalent to applying a lowpass filter to the resulting synthetic seismograms. Both single shots ($2.5*10^9$ Nt-m total explosion moment) and multiple shots ($1.0*10^{11}$ Nt-m total explosion moment) with ripple firing were simulated. Most simulations were run to between 3 and 4 seconds duration requiring between 48 and 72 hours of CPU time on an SGI R8000 workstation. Three components of velocity were saved on the free surface at every 160 or 640 m and every 0.01 or 0.04 sec. Several calculations were performed with the linear gradient velocity model (Table 3) instead of the original model of Bonner, *et al.* (1996) (shot_0a, shot_1c, and shot_1d). No

significant differences were seen in the results from the calculations with the linear gradients. One calculation (shot_1e) was performed with lower P velocities in the upper layers consistent with a Vp/Vs = 2 in order to test the sensitivity of the results upon the Poisson's ratio of the material. In order to test the sensitivity to the location of the shots behind the quarry face two locations were chosen for the single shots (see Figure 7). One calculation (shot_1d) was conducted with the explosion source 10 m behind the quarry face rather than 5 m behind the quarry face.

Table 6. 3D Finite Difference Calculations

Run	Quarry Present Quarry Face	Velocity Model	Multiple/Single Shot Shot Location	Burden
shot_0	No	Original	single	-
shot_0a	No	Linear Gradient	single	-
shot_0b	No	Linear Gradient with Vp/Vs=1.67 in upper layers	single	-
shot_1	Yes South	Original	multiple fired ripple west-to-east	5 m
shot_1a	Yes South	Original	single - location 1	5 m
shot_1b	Yes South	Original	single - location 2	5 m
shot_1c	Yes South	Linear Gradient	single - location 1	5 m
shot_1d	Yes South	Linear Gradient	single - location 2	10 m
shot_1e	Yes South	Linear Gradient with Vp/Vs=1.67 in upper layers	single - location 2	5 m

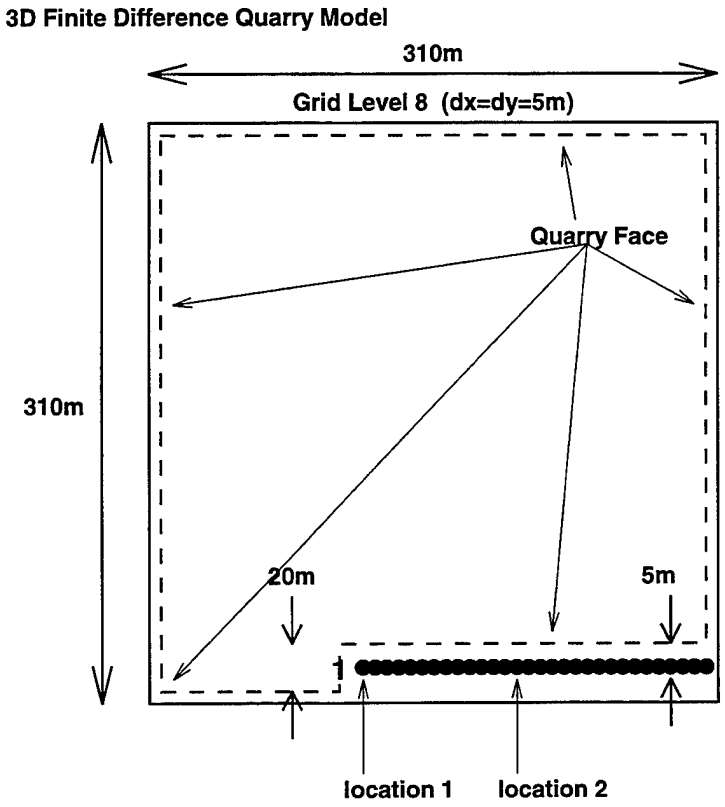

Figure 7. Diagram of quarry models and shot locations used to simulate 3D wave propagation. The line of multiple shots 5 m behind the bench is indicated by filled circles. Two single shot locations #1 and #2 are labeled.

A comparison of the single shot in the layered half-space without the quarry (shot_0a) is compared with wavenumber integration synthetics in Figure 8. The wavenumber integration synthetics have been convolved with the appropriate source time function and both sets of seismograms have been low-pass filtered at 3 and 2.5 Hz. The waveform comparison provides confidence that the finite difference calculations are performing as expected. Grid dispersion can be seen for frequencies above 2.5 Hz in the finite difference calculations.

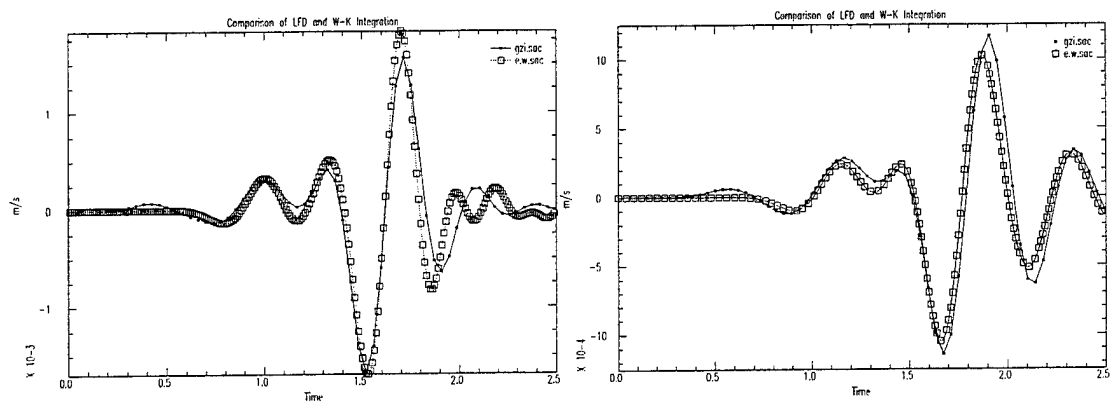

Figure 8. Comparisons of finite difference calculations for an explosion source in a layered half-space with wavenumber integration synthetics at a distance of 1000 m. The appropriate source time function has been convolved with the wavenumber integration green's explosion functions and all seismograms have been Low-pass filtered at 3.0 Hz (right) and 2.5 Hz (left).

2.8 Results of 3D Finite Difference Calculations

Snap shots of the vertical velocity and the total horizontal velocity are shown in Figure 9 for the shot_1 simulation. This calculation simulates the ripple fire of multiple shots 5 m behind a 10 m high bench. Phase reversals for waves radiated behind the bench are immediately evident. The total horizontal component contains both radial and transverse motion and the individual seismograms must be rotated before we can separate the P-SV and SH components of motion.

The rotated synthetic seismograms at a distance of 2 km from the multiple ripple simulation (shot_1) are shown in Figure 10. The seismograms have been low-pass filtered at 2 Hz. Surprisingly there are clear phase reversals of all three components for seismograms behind the bench (to the south) compared to seismograms across the quarry (to the north). The maxima of the envelope of each seismogram were measured and the radiation pattern for the vertical, radial and transverse components of motion are shown in Figure 11. Note that the vertical and radial components of motion are local maxima in directions perpendicular to the quarry face and motions are enhanced in the direction of the ripple fire. The transverse motion radiation pattern is aligned parallel to the quarry face and enhanced in the direction of ripple fire.

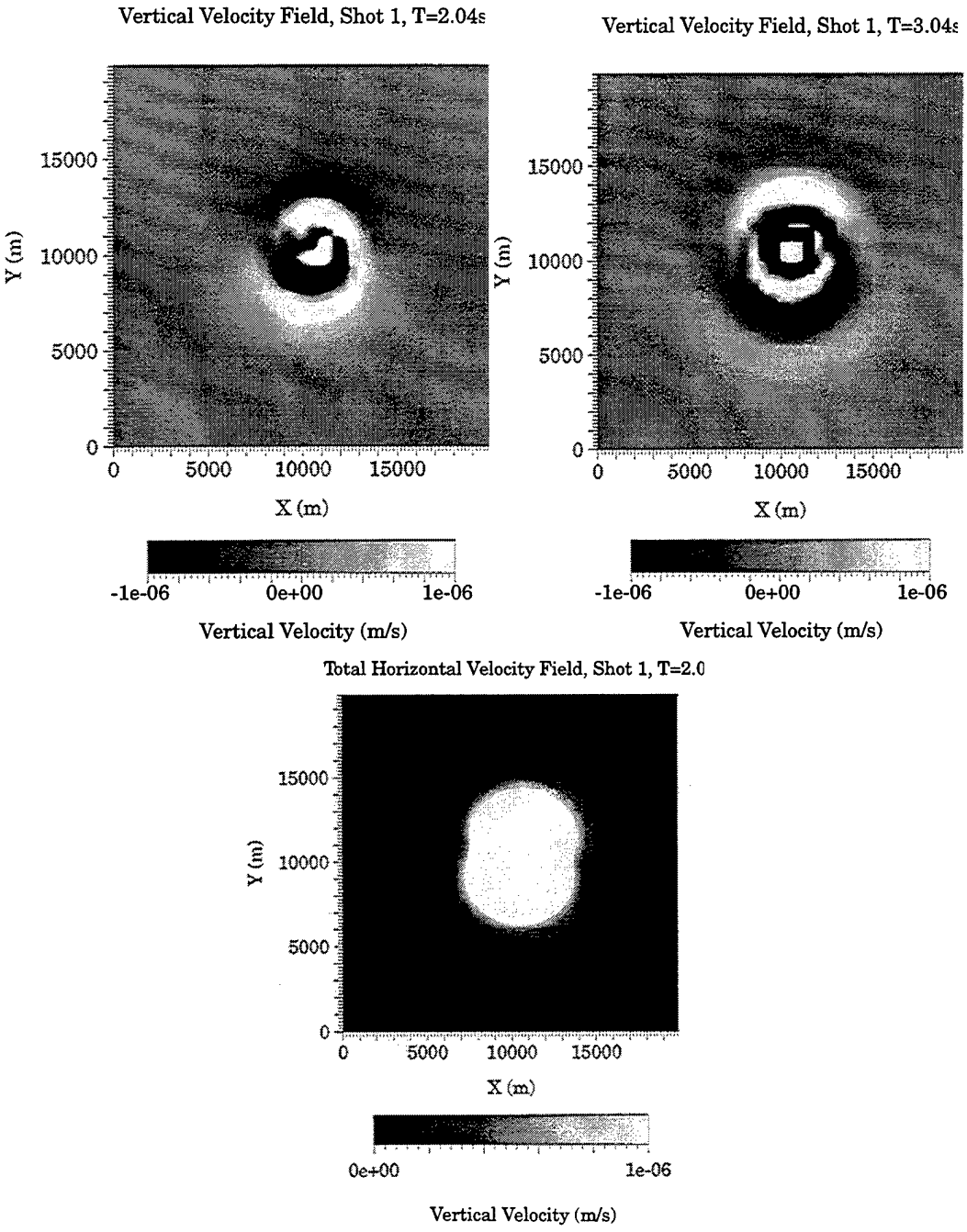

Figure 9. Snap shots of the vertical velocity from simulation shot_1 at T=3 sec. (top left) and T=2 sec. (top-right) and total horizontal velocity at T=2 2 sec. (bottom-center). Note the peanut-shaped radiation pattern for the total horizontal component and the phase reversals of the vertical component.

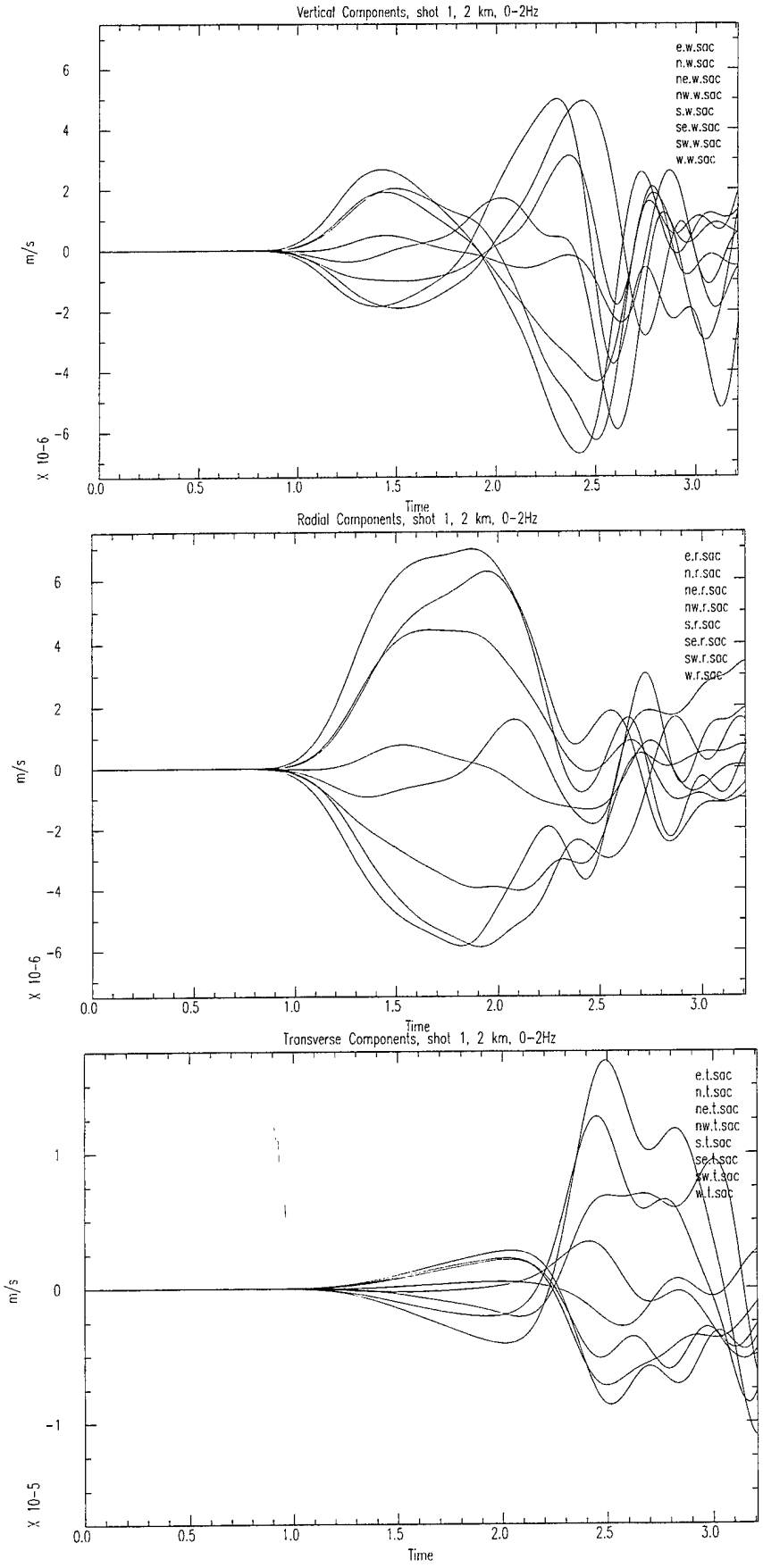

Figure 10. Vertical, radial, and transverse synthetic seismograms at a distance of 2 km from simulation shot_1. Seismograms have been lowpass filtered at 2 Hz.

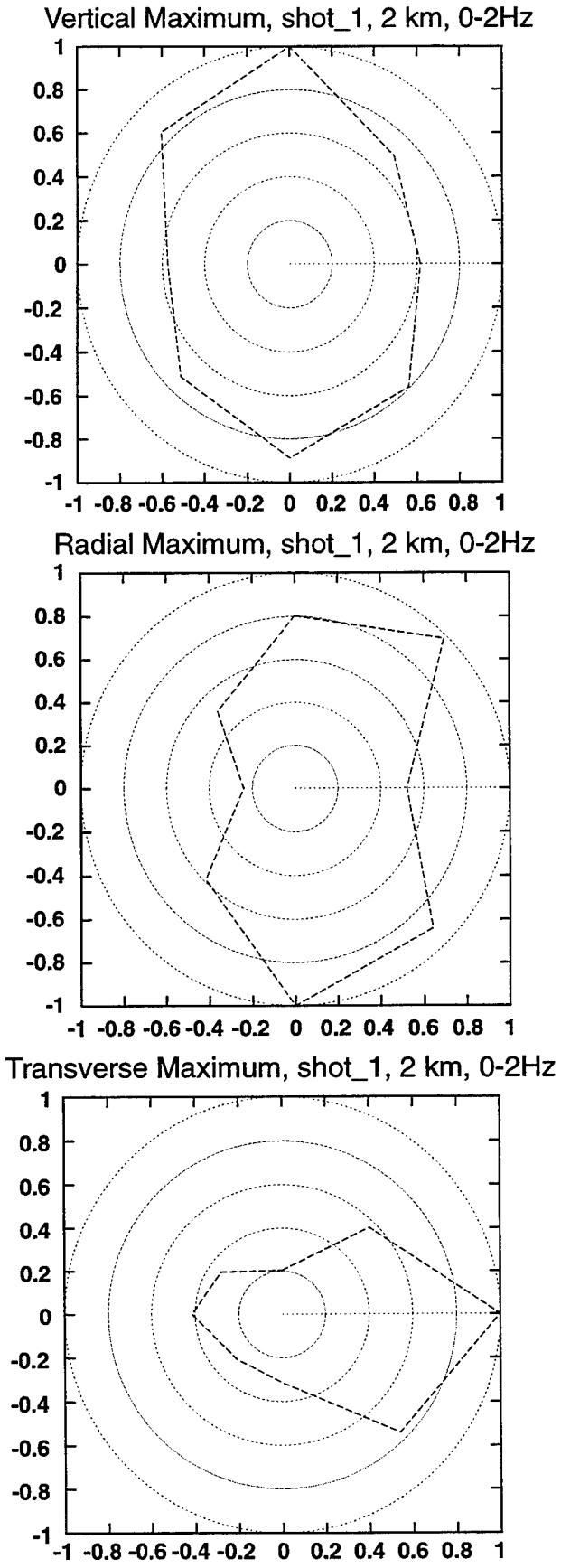

Figure 11. Radiation patterns are the maxima of the envelopes of the seismograms of Figure 10. shot_1, ripple fired.

In order to separate the effects of the ripple fire from the single shot and test the sensitivity of the radiation patterns upon location along the bench, we performed several single point explosion simulations listed in Table 6. It is easier to examine the individual phases of the point sources on the seismograms since they do not have the long source duration. Synthetic seismograms at a distance of 2 km from a single shot located 5 m behind an outside bench corner (shot_1a) are shown in Figure 12. The radiation patterns are shown in Figure 13.

We do not present detailed results for the simulations, shot_1b, shot_1c, shot_1d, and shot_1e. The point source simulations at location #2, shot_1b and shot_1d, did not show results significantly different from the shot_1a simulation demonstrating that the effect of the point source explosion behind the bench is not sensitive to the location along the bench and that the effect continues to a distance at least as far behind the bench as the bench is high. The simulations with linear velocity gradients, shot_0b, shot_1c and shot_1d, demonstrated that results are nearly identical to models without the velocity gradient for seismograms at 1, 2, and 4 km from the source. The fundamental Rayleigh and Love waves that dominate the seismograms in the 1 to 2 Hz bandwidth are not greatly sensitive to details of the velocity below 1 km at these distances. The simulation with a lower Vp/Vs ratio in the upper layers demonstrated that the results are not sensitive to the Poisson's ratio. The phase reversals are observed for Vp/Vs ratios between 2 and 3.

It is immediately obvious that the Love wave (SH or transverse) radiation patterns of Figures 11 and 13 are similar to the observed radiation patterns of Figure 3 when we account for the tendency for the patterns to be enhanced in the direction of the ripple fire. However, the P-SV (vertical and radial) radiation patterns of Figures 11 and 13 do not show the asymmetry of enhanced radiation behind the bench evident in Figure 3. From this comparison it is clear that the observed radiation patterns in Rg cannot be produced by the topographic bench alone. The observed enhancement of Rg behind the bench is much larger than can be explained by the topographic effects. Next, we examine the spall model.

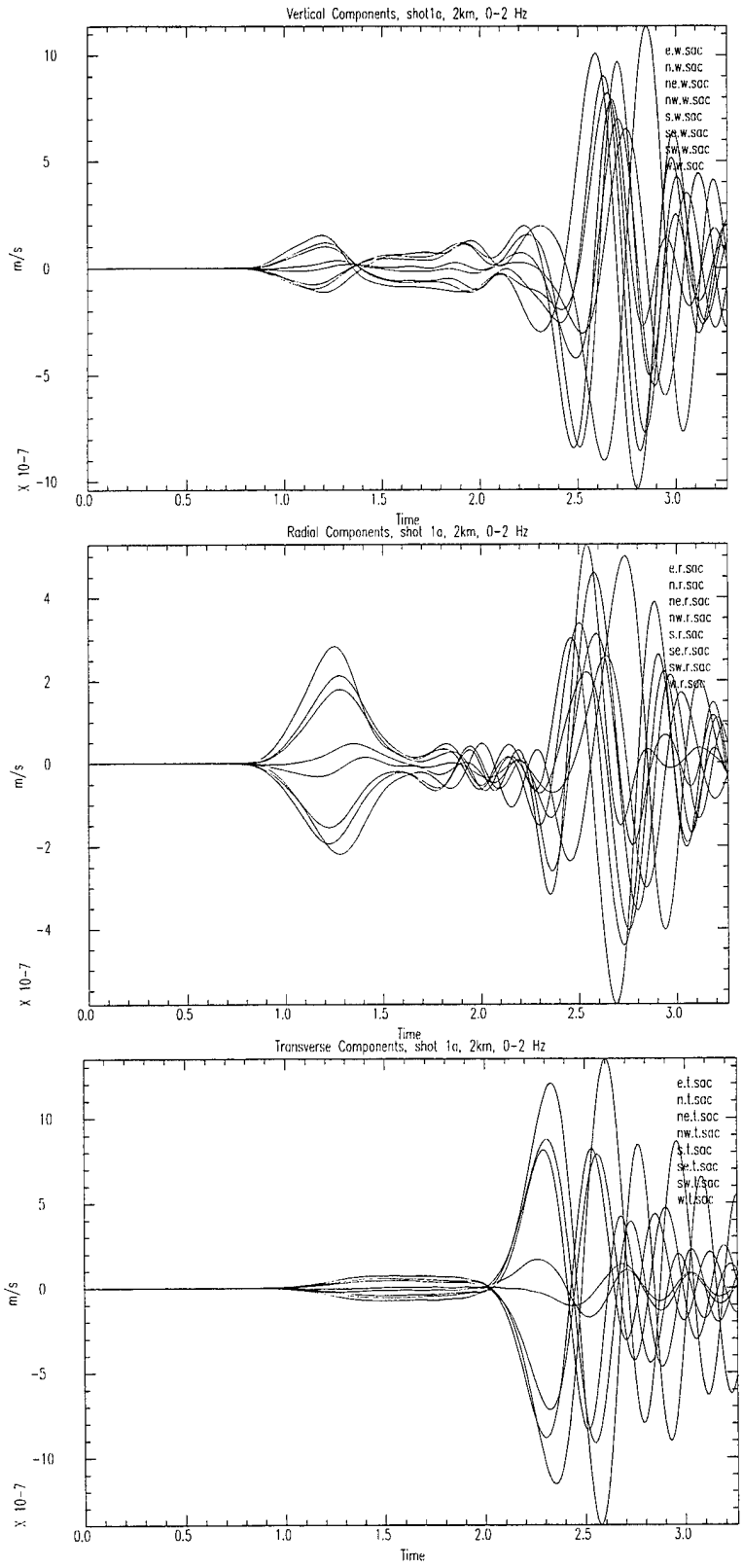

Figure 12. Vertical, radial, and transverse synthetic seismograms at a distance of 2 km from simulation shot_1a. Seismograms have been lowpass filtered at 2 Hz.

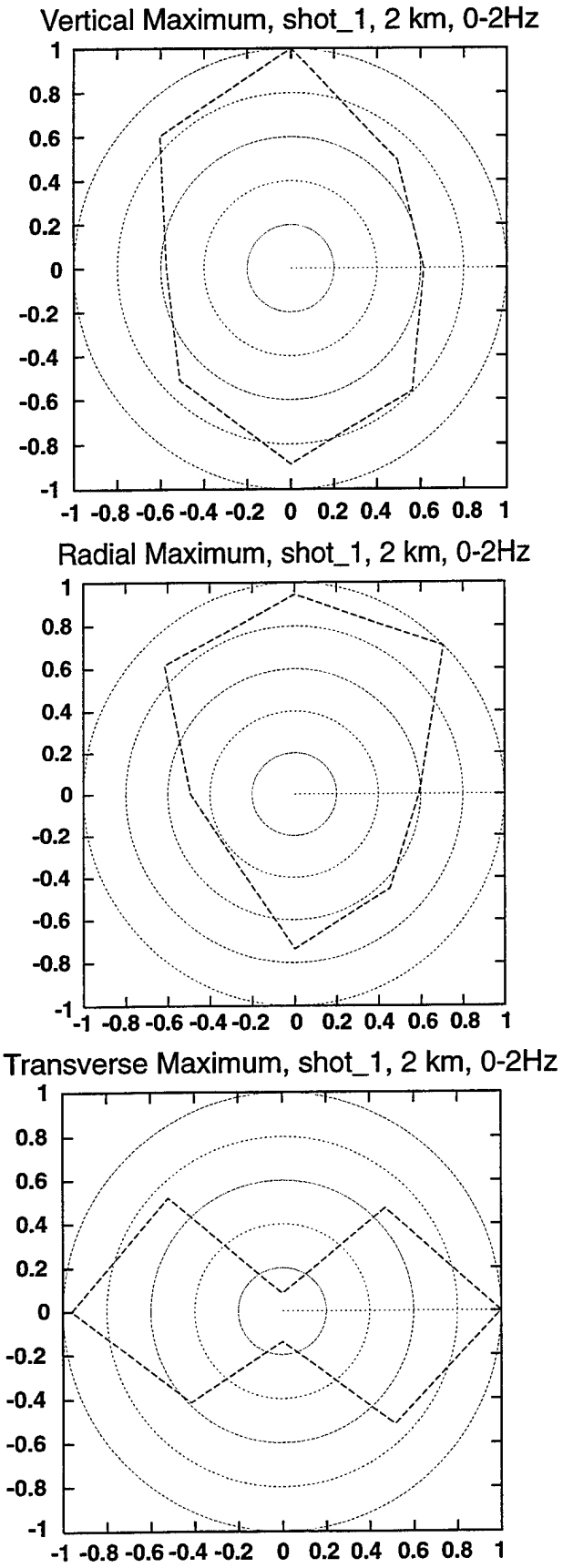

Figure 13. Radiation patterns are the maxima of the envelopes of the seismograms of Figure 12 shot_1a.

2.9 Modeling Spall with Wavenumber Integration Synthetics

We next attempted to model the observed radiation patterns with a simple explosion plus spall model of Barker, *et al.* (1993a). Green's functions were synthesized for the velocity model in Table 4 at a distance of 10 km. The explosion Green's functions were then convolved with a 1.1 second long boxcar with a total explosion moment of $M_0 = 3*10^{11}$ Nt-m. The vertical and horizontal force Green's functions were convolved with functions representing the time derivatives of the vertical and horizontal momentum of 20,000 metric tons of rock with a take-off velocity of 4.24 m/s at an angle of 45 degrees in the north direction. The spall functions were further convolved with a 1.1 second duration boxcar with unit area to represent the ripple duration. We assumed no net change in the height of center of mass of the material for the first model (spall_1) and assumed the center of mass fell one-half the height of the bench in a second model (spall_2).

The source functions are shown in Figure 13 and following Barker, *et. al.*, (1993a) we write the vertical, F_z, and horizontal, F_y, forces as

$$F_z = m[\dot{z}_0\delta(t) + (gt - \dot{z}_0)\delta(t - t_d) - g(H(t) - H(t - t_d))] \otimes [H(t) - H(t - t_r)] / (t_r - t)$$

and

$$F_y = m\dot{y}_0[\delta(t) - \delta(t - t_d)] \otimes [H(t) - H(t - t_r)] / (t_r - t)$$

where the spall dwell time is given by

$$t_d = [\dot{z}_0 + (\dot{y}_0^2 + 2z_0 g)^{1/2}] / g,$$

and the initial horizontal and vertical velocities are given by

$$(\dot{y}_0, \dot{z}_0) = V_0(\sin\theta, \cos\theta).$$

Note that the ripple duration spreads out the spall forces over time and the total spall duration is the sum of the spall dwell time and the ripple duration.

Table 7. Explosion Plus Spall Models

Model	Explosion Moment M_0 (Nt-m)	Ripple Duration t_r (sec)	Total Mass, m (metric ton)	Take-off Velocity, v_0 (m/s)	Take-off Angle, θ (degrees)	Elevation Change, z_0 (m)	Spall Dwell Time, t_d (sec)
spall_1	$3 * 10^{11}$	1.1	20,000	4.24	45	0	0.6
spall_2	$3 * 10^{11}$	1.1	20,000	4.24	45	5	0.9

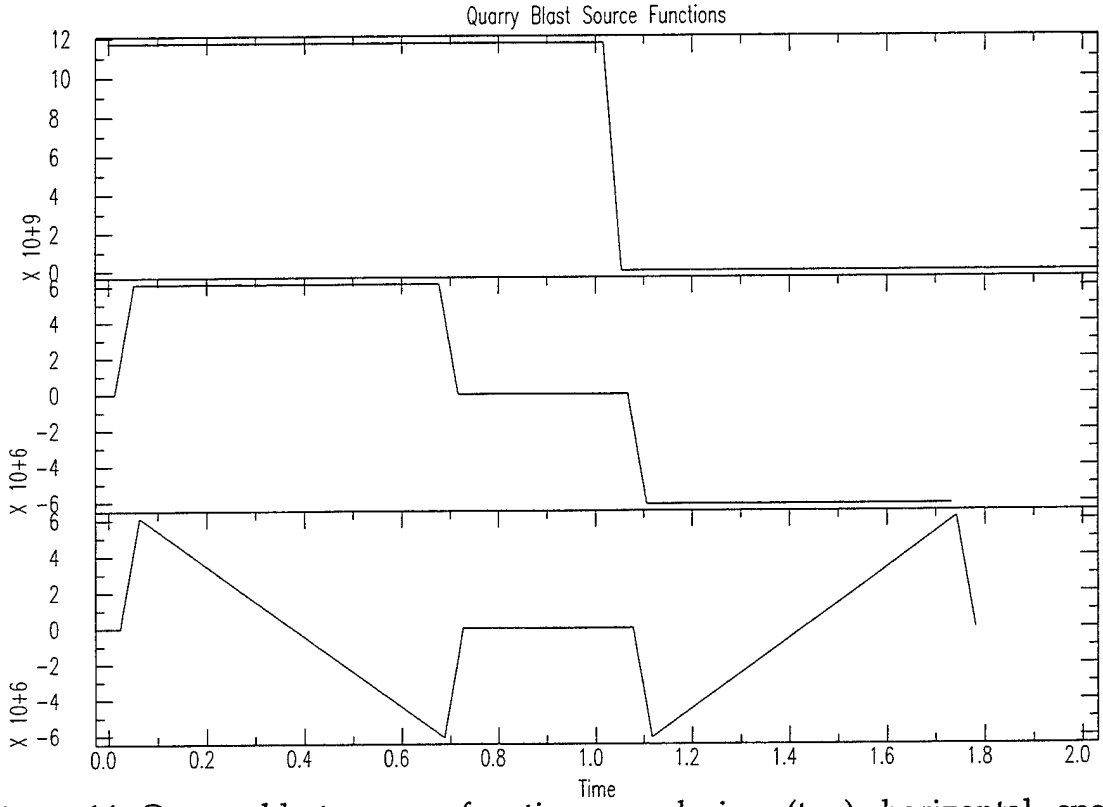

Figure 14. Quarry blast source functions: explosion (top), horizontal spall force (middle), and vertical spall force (bottom). Note that the total duration of the spall signal is the sum of ripple duration and spall dwell time.

Samples of the spall model seismograms and the radiation patterns are shown in Figures 15. It is clear that the largest phases on these seismograms are the fundamental Rayleigh and Love waves. Therefore, the maxima of the envelopes of the bandpassed synthetic seismograms were computed to form the radiation patterns seen in Figure 16. No attempt was made to simulate the spatial extent of the ripple fire (approximately 200 m long) upon the radiation patterns.

We can see from these seismograms that the approximate SV/SH amplitude ratios are consistent with observations that give maximum Rg/Love ratios perpendicular to the quarry face. Of coarse the spall model predicts a null perpendicular to the quarry face while observations favor a weak but measurable Love wave in that direction. Consistent with the central Texas observations, the P-SV (vertical and radial) amplitudes are maximum behind the bench, however the amplitude enhancement in the spall model is much less (about 25%) compared to the observations (about 300%). The asymmetry of the spall radiation pattern arises out of the interference of the horizontal force, the vertical force, and the explosion moment components of the source. The radiation patterns of the vertical force and the explosion are isotropic while the horizontal force introduces the asymmetry. It may be possible to further adjust the time functions of these three fundamental components of the source to better model the observed Rg radiation pattern asymmetry. We do not present the details of the second spall model (spall_2) except to say that with the source time functions of Barker, *et al.* (1992a) the introduction of a net fall in the center of mass did not greatly change the radiation patterns from those seen in Figure 16.

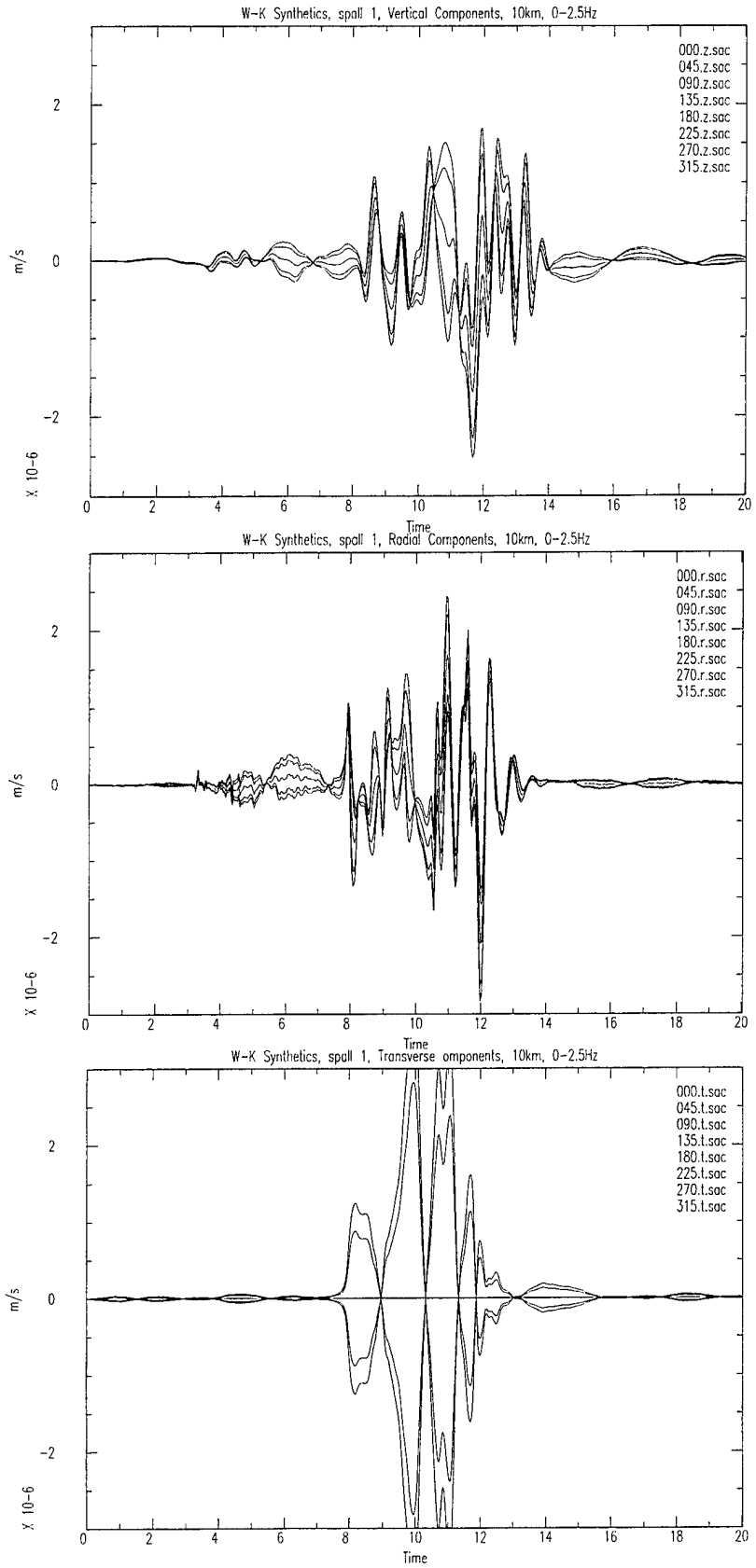

Figure 15. Seismograms derived from spall model 1.

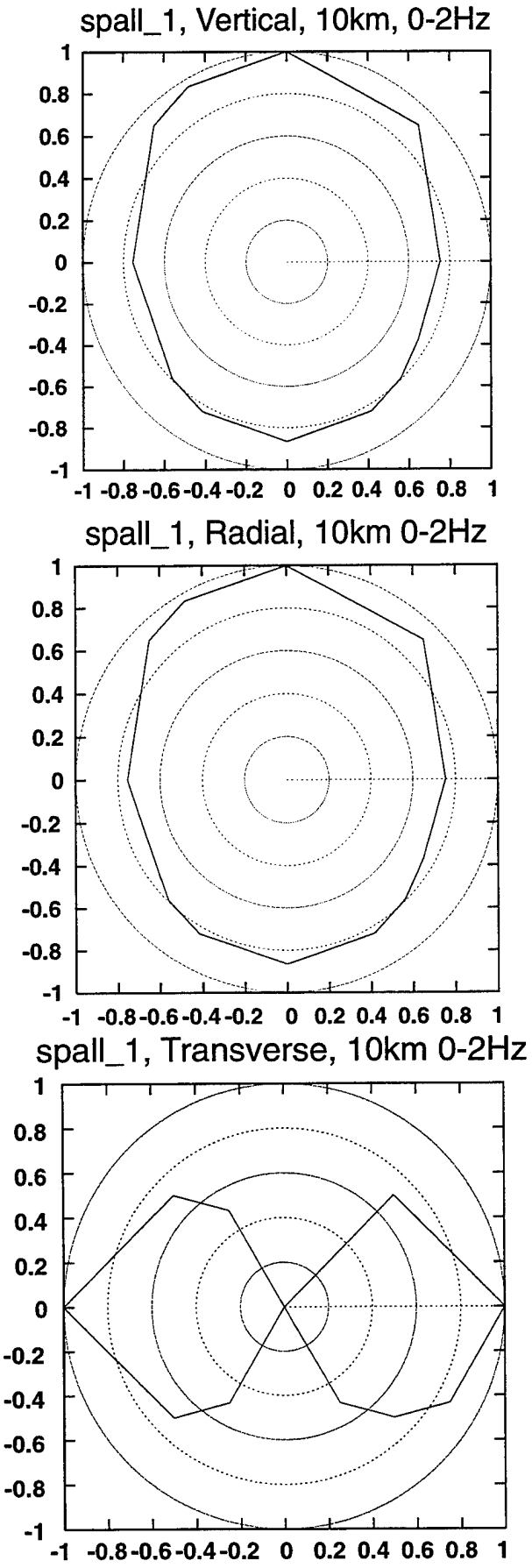

Figure 16. Radiation Patterns at 10 km, 0-2 Hz, for the Model Spall_1.

2.10 Modeling the Bench Face with a Moment Tensor Source

Barker, *et al.* (1993b) postulated that the effects of the bench upon the seismic radiation from a quarry blast explosion may be modeled by a modified moment tensor. They argued that the couple perpendicular to the quarry face will be effectively reduced by the presence of the free-surface boundary condition. Following this suggestion, we convolved the individual Green's function components for Mxx, Myy, and Mzz with 1.1 sec duration boxcars such that Myy = γ (Mxx = Mzz = M_0). Seismograms were computed for selected azimuths and the radiation patterns in Figure 17 were computed from the maxima of the envelopes of the bandpass filtered synthetic seismograms.

Table 8. Moment Tensor Model for the Explosion Behind the Bench

M_0 (Nt-m)	Ripple Duration (sec)	γ
$3*10^{11}$	1.1	0.2

We can see from these synthetic radiation patterns that the transverse (Love wave) radiation is a four-lobed pattern with nodes parallel and perpendicular to the quarry face. The maximum Love waves from such a source are at 45 degree azimuths to the quarry face. The vertical and radial synthetics are maximum perpendicular to the quarry face. These radiation patterns do not appear to reflect what we see from the 3D linear finite difference calculations. It is clear that the theoretical radiation from an explosion behind a bench is more complicated that the simple model suggested in Barker, *et al.* (1993b). The simple model of a reduced moment tensor component is not consistent with either the data or the more complete 3D finite difference calculations.

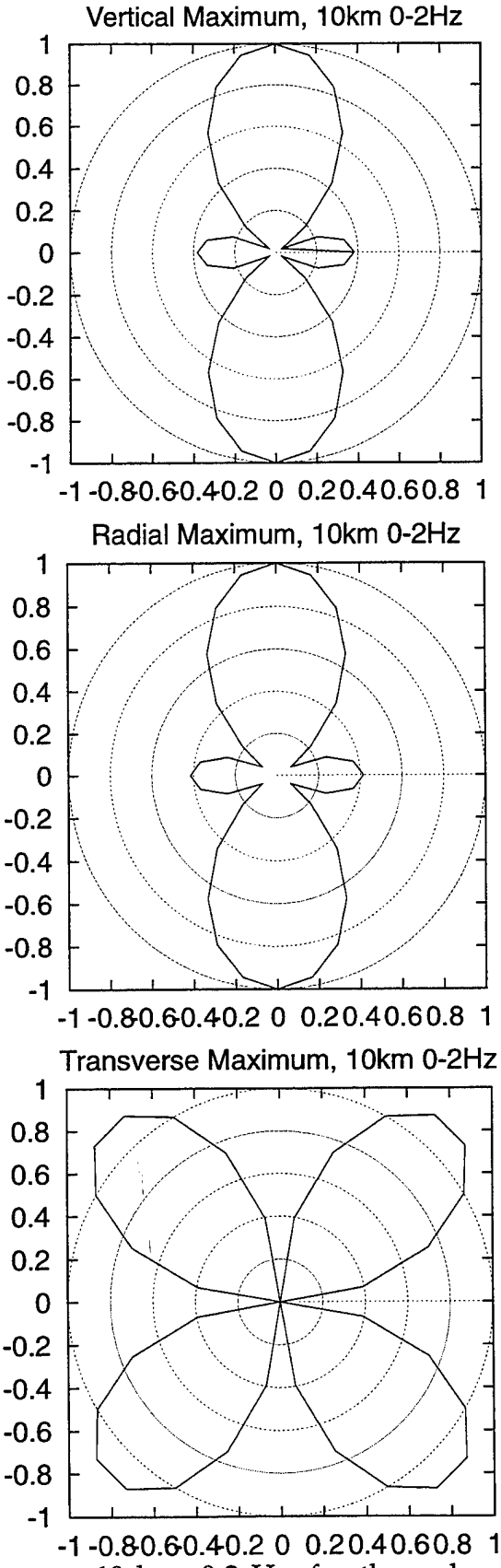

Figure 17. Radiation patterns at 10 km, 0-2 Hz, for the reduced moment tensor source, Myy = γ (Mxx = Mzz = M_0), γ = 0.2. This model neither represents the finite difference calculations nor the observed data.

2.11 Conclusions

We have attempted to model observed short-period fundamental Rayleigh (Rg) and Love (SH) waves from a quarry in central Texas at distances of about 10 km. Radiation patterns for the short period fundamental Rayleigh waves and Love waves are correlated with orientations of the quarry faces. Two physical based models have served as working hypotheses for the non-isotropic radiation from these quarry blasts. The first model assumes that the throw (spall) of material by the quarry blast can be modeled by simple forces applied to the horizontal free-surface (Barker, *et al.*, 1993a). The second hypothesis posits that non-planar free surfaces introduce non-isotropic radiation patterns into the regional waveforms (Barker, *et al.*, 1993b).

3D finite difference calculations show SV and SH radiation patterns roughly consistent with observations. However, we find that radiation patterns from an explosion behind the 3D bench are not represented by a modified moment tensor as suggested by Barker, *et al.* (1993b). Barker, *et al.* postulated that the effect of the quarry bench may be modeled by simple modification of the explosion moment tensor. The simple model of a reduced moment tensor component is not consistent with either the data or the more complete 3D finite difference calculations.

Preliminary modeling using plane-layered synthetics demonstrate that the magnitude of the SH compared to SV may be explained by the spall mechanism. Nearly all of the mass must participate in the spall with velocities of 2 to 5 m/s. Love wave radiation patterns are also consistent with such a mechanism. The Rg radiation patterns from an explosion plus a spall appear to differ somewhat from the observed pattern and may suggest that both the spall and free face are necessary to completely explain the azimuthal radiation patterns of both the Love and Rayleigh.

3. Modeling the Black Thunder Mine Data

3.1 Black Thunder Mine Series: Near Field Data

Data for three shots described in Stump, *et al.* (1996) were made available to us by Dr. Craig Pearson at LANL. The shots are two large ripple-fired cast shots, and a simultaneously detonated, contained coal shot (not cast). In Figure 18, we show the locations of the near-field recording sites relative to the cast shot done on Julian days 167 and 174 of 1996. Descriptions of the sensors can be found in Stump, *et al.* (1996). The plot shows the location of the pit (stippled area) at the time of these shots. Mining operations have proceeded from north to south, and the land is reclaimed after coal is removed. Thus, the highwall is on the south side of the pit. The cast blasts originated at the same location, with shot 167 (4.7 million lbs) propagating to the right, ending at the edge of the pit, and shot 174 (2.3 million lbs) propagating to the left. The material was thrown to the NE by shot 167 and to the NW by shot 174. The coal shot (day 236) is west of shot 167.

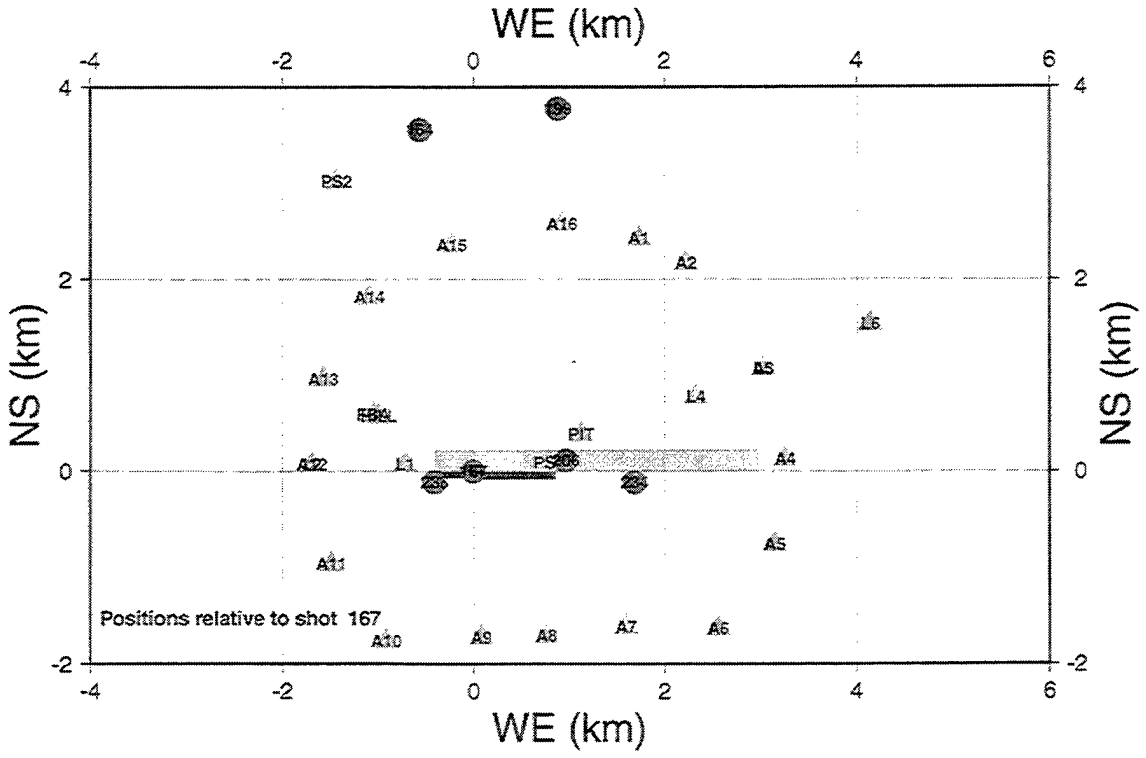

Figure 18. Locations of shots (circles) and recorders (triangles) relative to shot 167. The pit is shown as the stippled area.

We have focused on two aspects of the data: the differences between the coal and cast blasts and the azimuthal patterns. Coal shots are used to bulk (fracture) material prior to removal. This is accomplished by exploding vertical shot holes which cause the material to lift and drop, with little horizontal movement. These shots are usually ripple fired to minimize ground roll, but shot 236 was shot simultaneously, especially for this experiment. The cast shots are the standard ripple-fired, distributed shots which cast material horizontally from the highwall into the pit. Thus, the primary differences in coal and cast blasts from the point of view of this program are:

1. The coal shots have no horizontal movement and very little net vertical movement, while the cast shots have both. The effects of mass movement on seismic signals was investigated theoretically by Barker, *et al.* (1995). The horizontal motion produces a horizontal force in the direction of the mass movement, and a corresponding radiation pattern. The duration of vertical motion causes band-limited signals peaked between 0.2 and 1 Hz.
2. The coal shot (in this case) is localized temporally and spatially, while the cast shots are distributed. The finite duration of the signal (usually several seconds) has the effect of low-pass filtering the data with a corner frequency that is the inverse of the duration.
3. The cast shots occur on the side of the face to be removed, while the coal shot was detonated in the bottom of the pit. The geometrical effects have been studied in the numerical experiments discussed in Section II and in Barker, *et al.* (1994).

To investigate the role of the source time history, we convolved the firing pattern of the ripple-fired cast blasts with the simultaneously detonated coal shot. If there are no geometrical effects or effects due to mass movement, then the convolved results should match the cast shots. That is, if the firing pattern of the cast blast is $F_{cast}(t)$, the seismogram from the cast blast is $S_{cast}(t)$, and the seismogram if the coal shot is $S_{coal}(t)$, then we would have $S_{cast}(t) = S_{coal}(t) * F_{cast}(t)$. In Figure 19, we show the convolutions and seismograms for both cast blasts (167 and 174) at station A6. It can be seen that the firing pattern accounts for many of the differences between the coal and cast blasts, in particular the signal duration and peak amplitude. When recordings from other shots in the series become available, it will be possible to be more quantitative.

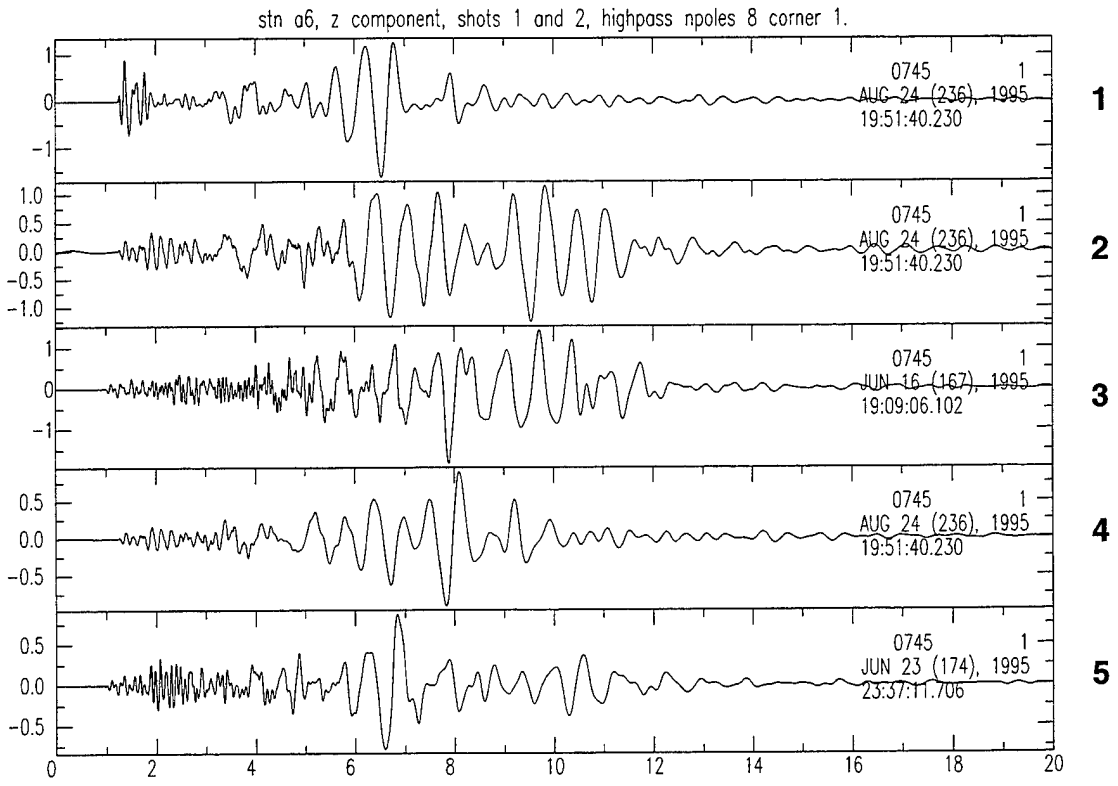

Figure 19. Time series from top-to-bottom are (1) the coal shot, (2) the coal shot convolved with the firing pattern for cast blast 167, (3) cast blast 167, (4) the coal shot convolved with the firing pattern for cast blast 174, and (5) cast blast 174.

The primary objective in examining the azimuthal patterns from these shots is to infer the source radiation pattern, and from that, a source model. Figure 20 shows the radiation patterns of the vertical, radial and tangential components from shots 167 and 174 recorded at the "A" stations (Figure 18). Plotted are the peak amplitudes in the band from 1 to 3 Hz, which are typically found in the Rayleigh wave (see the seismograms in Figure 19). The station labels are shaded differently to indicate whether they are on reclaimed land (stations A1 to A4 and A14, A15) or unmined land (stations A5 to A13). Generally, smaller amplitudes are associated with reclaimed land and larger amplitudes are associated with unmined land. Also shown on each figure are the site response radiation patterns at the stations as estimated by the spectral amplitude of the coda. At each station, the spectrum of the coda (starting at about 14 seconds into the records shown in Figure 19) is averaged from 1 and 3 Hz, then averaged between the two shots, and plotted (after normalization to the maximum) versus azimuth. If variations in azimuth were due solely to site response (and the coda is a good estimate of the response), then the azimuthal patterns of signal and coda response would be the same, and we could attribute the differences to source radiation. The coda response for the

vertical component is largest to the SSE, and so is the peak motion for shot 167. However, the vertical motion from shot 174 has a pattern which is larger to the SW, which indicates a difference in vertical source radiation. Recall that these two shots were different in their total yield and in the throw direction, with 167 NE and 174 to the NW. If there are directivity effects, we would expect them to be in the direction of the throw, which is not observed. We would also expect geometrical effects associated with the quarry to be about the same since they were shot from the same place on the same highwall. The spall of material can be modeled by vertical and horizontal forces applied to the free surface with time functions proportional to the derivative of the momentum of the spalled material (e.g., Barker, *et al.*, 1993a). The models predict dipolar patterns in the radial and transverse components, elongated in the direction of throw for the radial and perpendicular to the throw for the transverse component. This is also not observed.

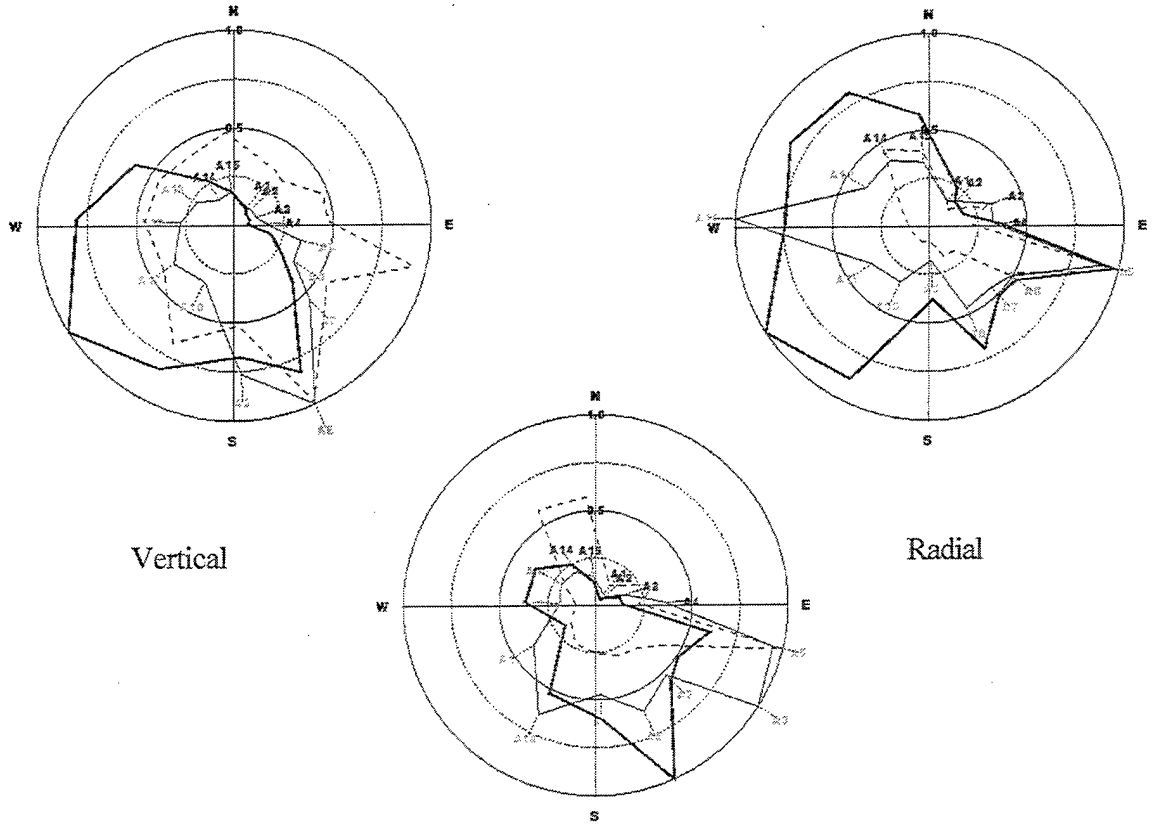

Figure 20. Radiation patterns of narrow band peak amplitude (1 to 3 Hz) for shot 167 (lighter line), shot 174 (heavier line) and coda response (dashed line) for three components of motion.

We conclude that near-field recordings are heavily contaminated by path and site effects. Further progress awaits additional data we have requested from LANL which may provide insight into the site response. Those data are recordings at these sites of events occurring outside the mine, within the Powder River Basin and beyond. We plan to determine local site response using coda techniques often employed in earthquake research (e.g. Van de Vragt, *et al.*, 1996) in order to better separate source and propagation effects.

3.2 Black Thunder Mine Series: Regional Data

In addition to studies of the near-field data described above, we have begun analyses of near-regional data presented by Hedlin, *et al.*, (1996). In the summer of 1996, IGPP/UCSD deployed five seismometers at ranges between 100 and 200 km from the Black Thunder mine, which augment the permanent regional stations RSSD and PDAR. To determine path properties to these sites, we extracted Rayleigh wave dispersion curves and inverted them for earth structure using signals from three shots. Figure 21 shows the shear wave structures derived for each site.

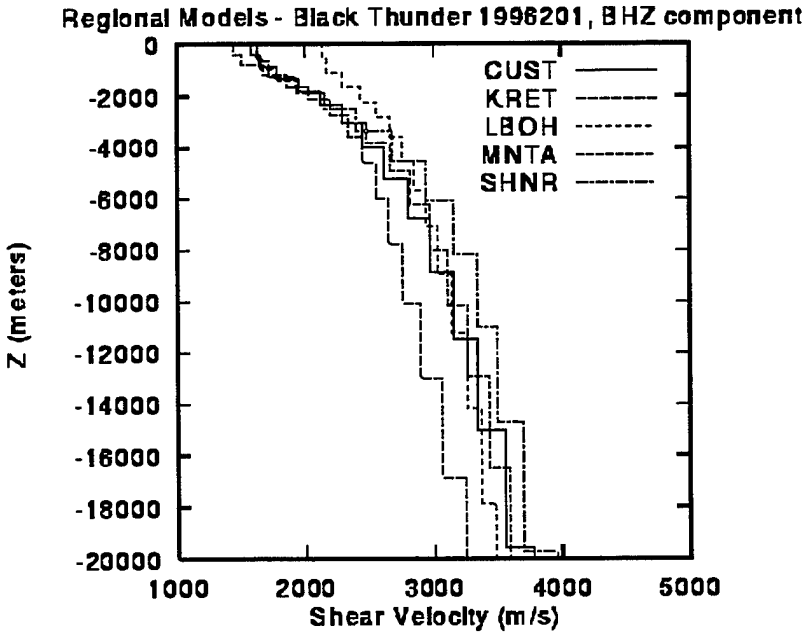

Figure 21. Shear velocity structure at four sites from the shot on Julian day 1996201.

The models are quite consistent, with the exception of LBOH. These sites are all within the Powder River and Wind River Basins, except LBOH, to which signals must cross the Black Hills pluton.

Hedlin, *et al.* (1996) recorded three large blasts, two in the South Pit (see Figure 18) and one in the North Pit. During one of the South Pit shots, a large fraction of the holes detonated simultaneously (unintentionally). The Rayleigh wave spectra, corrected for propagation by using phase velocities as phase matched filters, are shown in Figure 22 for station MNTA (Δ=204 km, azimuth=254^0). The spectra for shots 215 and 201 (in the South Pit) are quite similar across the band, in spite of the simultaneous part of the detonation in shot 215. Shot 201, in the North Pit, has the largest difference in amplitude at low frequencies indicating source location is a stronger effect on amplitude than firing pattern.

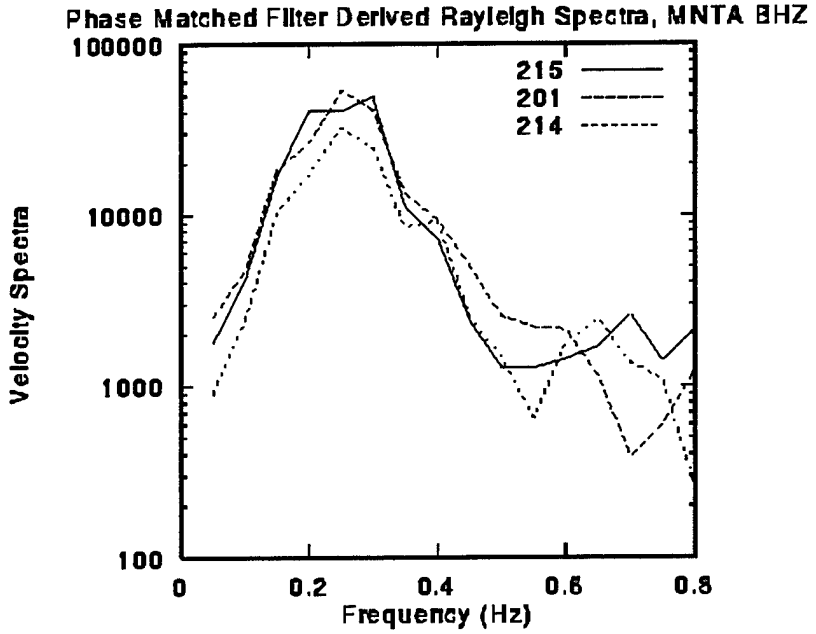

Figure 22. Rayleigh wave spectra from three Black Thunder shots recorded at MNTA

4. Conclusions

We have attempted to model observed short-period fundamental Rayleigh (Rg) and Love (SH) waves from a quarry in central Texas at distances of about 10 km. Radiation patterns for the short period fundamental Rayleigh waves and Love waves are correlated with orientations of the quarry faces. Two physical based models have served as working hypotheses for the non-isotropic radiation from these quarry blasts. The first model assumes that the throw (spall) of material by the quarry blast can be modeled by simple forces applied to the horizontal free-surface (Barker, *et al.*, 1993a). The second hypothesis posits that non-planar free surfaces introduce non-isotropic radiation patterns into the regional waveforms (Barker, *et al.*, 1993b).

3D finite difference calculations show SV and SH radiation patterns roughly consistent with observations. However, we find that radiation patterns from an explosion behind the 3D bench are not represented by a modified moment tensor as suggested by Barker, *et al.* (1993b). Barker, *et al.* postulated that the effect of the quarry bench may be modeled by simple modification of the explosion moment tensor. The simple model of a reduced moment tensor component is not consistent with either the data or the more complete 3D finite difference calculations.

Preliminary modeling using plane-layered synthetics demonstrate that the magnitude of the SH compared to SV may be explained by the spall mechanism. Nearly all of the mass must participate in the spall with velocities of 2 to 5 m/s. Love wave radiation patterns are also consistent with such a mechanism. The Rg radiation patterns from an explosion plus a spall appear to differ somewhat from the observed pattern and may suggest that both the spall and free face are necessary to completely explain the azimuthal radiation patterns of both the Love and Rayleigh.

We observe strong variations in near field ground motions at the Black Thunder mine. Using estimates of site response derived from signal coda , we find that the variations are partly due to local structure. However, variations between nearly co-located shots indicate changes are also due to source mechanism. The data set provided to us at this time does not include all the data taken for these shots and it is anticipated that source and propagation effects can be resolved with the full data set.

5. References

Barker, T. G., K. L. McLaughlin, and J. L. Stevens (1996), "Physical Mechanisms of Quarry Blast Sources," *Proceedings of the 18th Annual Seismic Research Symposium on Monitoring a Comprehensive Test Ban Treaty*, edited by J. F. Lewkowicz, J. M. McPhetres and D. T. Reiter, Annapolis MD, PL-TR-96-2153, ADA313692.

Barker, T. G., K. L. McLaughlin, and J. L. Stevens (1993a), "Numerical Models of Quarry Blast Sources," S-CUBED Report SSS-TR-93-13859.

Barker, T. G., K. L. McLaughlin, J. L. Stevens and S. M. Day (1993b), "Numerical Models of Quarry Blast Sources: the Effects of the Bench," S-CUBED Semiannual Report to Phillips Laboratory, SSS-TR-93-13915.

Bonner, J., E. Herrin and T. Goforth, 1996, "Azimuthal Variation of Rg Energy in Central Texas," submitted to *Bull. Seism. Soc. Am.*

Bonner, J., E. Herrin, and T. Goforth (1996), "Azimuthal Variation of Rg Energy in Central Texas," submitted to SRL.

Day, S. M. and K. L. McLaughlin (1991), "Seismic Source Representations for Spall," *Bull. Seism. Soc. Am., 81,* 191-201.

Delitsyne, L., (1996), "Generation of Shear Waves from Quarries from Near-Regional Data," *Seis. Res. Lett. 67, #2,* 36.

Gitterman, Y, and T. van Eck (1993), "Spectra of Quarry Blasts and Microearthquakes Recorded at Local Distances in Israel," *Bull. Seism. Soc. Am., 83,* 1799-1812.

Goforth, T., and J. Bonner (1995), "Characteristics of Rg Waves Recorded in Central Texas," *Bull. Seism. Soc. Am. 85,* 1232-1235.

Harris, D. (1991), "A Waveform Correlation Method for Identifying Quarry Explosions," *Bull. Seism. Soc. Am., 81,* 2395-2418.

Hedlin, M., J. B. Minster, and J. A. Orcutt (1990), "An automatic means to discriminate between earthquakes and quarry blasts," *Bull. Seism. Soc. Am., 80,* 2143-2160.

Hedlin, M. A. H., F. L. Vernon, J. B. Minster and J.A. Orcutt (1996), "Experiments in Regional Monitoring of Small Seismic/Acoustic Events," *Proceedings of the 18th Annual Seismic Research Symposium on Monitoring a Comprehensive Test Ban Treaty,* edited by J. F. Lewkowicz, J. M. McPhetres and D. T. Reiter, Annapolis MD, PL-TR-96-2153, ADA313692.

Konya and Walter (1990), *Surface Blast Design*, Prentice Hall, 303 Pages.

Langefors, U. and B. Kihlstrom (1963), "The Modern Technique of Rock Blasting," John Wiley and Sons, New York, 405 pages.

McLaughlin, K. L. and S. M. Day (1994), "3D Finite Difference Modeling of Seismic Wave Propagation," *Computers in Physics*, Nov-Dec 1994.

McLaughlin, K. L., T. G. Barker and J. L. Stevens (1994), "Numerical Simulation of Quarry Blast Sources," S-CUBED Final Report to Phillips Laboratory, Kirtland AFB, SSS-TR-94-14418.

McLaughlin, K. L., J. Bonner and T. G. Barker (1996), "Seismic Source Mechanisms for Quarry Blasts Observed Rayleigh and Love Wave Radiation Patterns from a Texas Quarry," in preparation.

Prewitt, R.H., 1969, "Crustal Thickness in Central Texas as Determined by Rayleigh Wave Dispersion," [MS Thesis] Lubbock, Texas, Texas Tech. University.

Smith, A. T. (1989), "High-Frequency Seismic Observations and Models of Chemical Explosions: Implications for the Discrimination of Ripple-Fired Mining Blasts," *Bull. Seism. Soc. Am., 79*, 1089-1110.

Smith, A. T. (1993), "Discrimination of Explosions from Simultaneous Mining Blasts," *Bull. Seism. Soc. Am., 83*, 160-179.

Stump, B. W. and R. E. Reinke (1988), "Experimental Confirmation of Superposition from Small-Scale Explosions," *Bull. Seism. Soc. Am., 78*, 1059-1073

Stump, B. W., D. C. Pearson, R. L. Martin, P. E. Harben, C. L. Edwards, D. Baker, K. Kihara, K. Dalrymple, J. P. Lewis, D. Rock and R. Boyd, "The Black Thunder Regional Seismic Experiment," LANL Report LAUL-95-3980.

Su, F., K. Aki, and N. Biswas (1991), "Discriminating Quarry Blasts from Earthquakes Using Coda Waves," *Bull. Seism. Soc. Am.*, 162-178.

Willis, D. E. (1963), "A Note on the Ripple-Firing on Spectra of Quarry Blasts," *Bull. Seism. Soc. Am., 53*, 79-86.

THOMAS AHRENS
SEISMOLOGICAL LABORATORY 252-21
CALIFORNIA INSTITUTE OF TECHNOLOGY
PASADENA, CA 91125

RALPH ALEWINE
NTPO
1901 N. MOORE STREET, SUITE 609
ARLINGTON, VA 22209

SHELTON ALEXANDER
PENNSYLVANIA STATE UNIVERSITY
DEPARTMENT OF GEOSCIENCES
537 DEIKE BUILDING
UNIVERSITY PARK, PA 16801

MUAWIA BARAZANGI
INSTITUTE FOR THE STUDY OF THE CONTINENTS
3126 SNEE HALL
CORNELL UNIVERSITY
ITHACA, NY 14853

T.G. BARKER
MAXWELL TECHNOLOGIES
8888 BALBOA AVE.
SAN DIEGO, CA 92123-1506

DOUGLAS BAUMGARDT
ENSCO INC.
5400 PORT ROYAL ROAD
SPRINGFIELD, VA 22151

THERON J. BENNETT
MAXWELL TECHNOLOGIES
11800 SUNRISE VALLEY DRIVE SUITE 1212
RESTON, VA 22091

WILLIAM BENSON
NAS/COS
ROOM HA372
2001 WISCONSIN AVE. NW
WASHINGTON, DC 20007

JONATHAN BERGER
UNIVERSITY OF CA, SAN DIEGO
SCRIPPS INSTITUTION OF OCEANOGRAPHY IGPP, 0225
9500 GILMAN DRIVE
LA JOLLA, CA 92093-0225

ROBERT BLANDFORD
AFTAC
1300 N. 17TH STREET
SUITE 1450
ARLINGTON, VA 22209-2308

STEVEN BRATT
NTPO
1901 N. MOORE STREET, SUITE 609
ARLINGTON, VA 22209

RHETT BUTLER
IRIS
1200 NEW YORK AVE., NW
SUITE 800
WASHINGTON, DC 20005

LESLIE A. CASEY
DOE
1000 INDEPENDENCE AVE. SW
NN-20
WASHINGTON, DC 20585-0420

CATHERINE DE GROOT-HEDLIN
UNIVERSITY OF CALIFORNIA, SAN DIEGO
INSTITUTE OF GEOPHYSICS AND PLANETARY PHYSICS
8604 LA JOLLA SHORES DRIVE
SAN DIEGO, CA 92093

STANLEY DICKINSON
AFOSR
110 DUNCAN AVENUE, SUITE B115
BOLLING AFB
WASHINGTON, D.C. 20332-001

DIANE I. DOSER
DEPARTMENT OF GEOLOGICAL SCIENCES
THE UNIVERSITY OF TEXAS AT EL PASO
EL PASO, TX 79968

RICHARD J. FANTEL
BUREAU OF MINES
DEPT OF INTERIOR, BLDG 20
DENVER FEDERAL CENTER
DENVER, CO 80225

MARK D. FISK
MISSION RESEARCH CORPORATION
735 STATE STREET
P.O. DRAWER 719
SANTA BARBARA, CA 93102-0719

ROBERT GEIL
DOE
PALAIS DES NATIONS, RM D615
GENEVA 10, SWITZERLAND

LORI GRANT
MULTIMAX, INC.
311C FOREST AVE. SUITE 3
PACIFIC GROVE, CA 93950

HENRY GRAY
SMU STATISTICS DEPARTMENT
P.O. BOX 750302
DALLAS, TX 75275-0302

DAVID HARKRIDER
PHILLIPS LABORATORY
EARTH SCIENCES DIVISION
29 RANDOLPH ROAD
HANSCOM AFB, MA 01731-3010

THOMAS HEARN
NEW MEXICO STATE UNIVERSITY
DEPARTMENT OF PHYSICS
LAS CRUCES, NM 88003

DONALD HELMBERGER
CALIFORNIA INSTITUTE OF TECHNOLOGY
DIVISION OF GEOLOGICAL & PLANETARY SCIENCES
SEISMOLOGICAL LABORATORY
PASADENA, CA 91125

ROBERT HERRMANN
ST. LOUIS UNIVERSITY
DEPARTMENT OF EARTH & ATMOSPHERIC SCIENCES
3507 LACLEDE AVENUE
ST. LOUIS, MO 63103

ANTHONY IANNACCHIONE
BUREAU OF MINES
COCHRANE MILL ROAD
PO BOX 18070
PITTSBURGH, PA 15236-9986

THOMAS JORDAN
MASSACHUSETTS INSTITUTE OF TECHNOLOGY
EARTH, ATMOSPHERIC & PLANETARY SCIENCES
77 MASSACHUSETTS AVENUE, 54-918
CAMBRIDGE, MA 02139

LAWRENCE LIVERMORE NATIONAL LABORATORY
ATTN: TECHNICAL STAFF (PLS ROUTE)
PO BOX 808, MS L-221
LIVERMORE, CA 94551

LAWRENCE LIVERMORE NATIONAL LABORATORY
ATTN: TECHNICAL STAFF (PLS ROUTE)
PO BOX 808, MS L-208
LIVERMORE, CA 94551

LAWRENCE LIVERMORE NATIONAL LABORATORY
ATTN: TECHNICAL STAFF (PLS ROUTE)
PO BOX 808, MS L-195
LIVERMORE, CA 94551

I. N. GUPTA
MULTIMAX, INC.
1441 MCCORMICK DRIVE
LARGO, MD 20774

IAN MACGREGOR
NSF
4201 WILSON BLVD., ROOM 785
ARLINGTON, VA 22230

MICHAEL HEDLIN
UNIVERSITY OF CALIFORNIA, SAN DIEGO
SCRIPPS INSTITUTION OF OCEANOGRAPHY IGPP, 0225
9500 GILMAN DRIVE
LA JOLLA, CA 92093-0225

EUGENE HERRIN
SOUTHERN METHODIST UNIVERSITY
DEPARTMENT OF GEOLOGICAL SCIENCES
DALLAS, TX 75275-0395

VINDELL HSU
HQ/AFTAC/TTR
1030 S. HIGHWAY A1A
PATRICK AFB, FL 32925-3002

RONG-SONG JIH
HQ DSWA/PMP/CTBT
6801 TELEGRAPH ROAD
ALEXANDRIA, VA 22310-3398

LAWRENCE LIVERMORE NATIONAL LABORATORY
ATTN: TECHNICAL STAFF (PLS ROUTE)
PO BOX 808, MS L-200
LIVERMORE, CA 94551

LAWRENCE LIVERMORE NATIONAL LABORATORY
ATTN: TECHNICAL STAFF (PLS ROUTE)
LLNL
PO BOX 808, MS L-175
LIVERMORE, CA 94551

LAWRENCE LIVERMORE NATIONAL LABORATORY
ATTN: TECHNICAL STAFF (PLS ROUTE)
PO BOX 808, MS L-202
LIVERMORE, CA 94551

LAWRENCE LIVERMORE NATIONAL LABORATORY
ATTN: TECHNICAL STAFF (PLS ROUTE)
PO BOX 808, MS L-205
LIVERMORE, CA 94551

THORNE LAY
UNIVERSITY OF CALIFORNIA, SANTA CRUZ
EARTH SCIENCES DEPARTMENT
EARTH & MARINE SCIENCE BUILDING
SANTA CRUZ, CA 95064

DONALD A. LINGER
DNA
6801 TELEGRAPH ROAD
ALEXANDRIA, VA 22310

LOS ALAMOS NATIONAL LABORATORY
ATTN: TECHNICAL STAFF (PLS ROUTE)
PO BOX 1663, MS F665
LOS ALAMOS, NM 87545

LOS ALAMOS NATIONAL LABORATORY
ATTN: TECHNICAL STAFF (PLS ROUTE)
PO BOX 1663, MS C335
LOS ALAMOS, NM 87545

KEITH MCLAUGHLIN
MAXWELL TECHNOLOGIES
8888 BALBOA AVE.
SAN DIEGO, CA 92123-1506

RICHARD MORROW
USACDA/IVI
320 21ST STREET, N.W.
WASHINGTON, DC 20451

JAMES NI
NEW MEXICO STATE UNIVERSITY
DEPARTMENT OF PHYSICS
LAS CRUCES, NM 88003

PACIFIC NORTHWEST NATIONAL LABORATORY
ATTN: TECHNICAL STAFF (PLS ROUTE)
PO BOX 999, MS K6-48
RICHLAND, WA 99352

PACIFIC NORTHWEST NATIONAL LABORATORY
ATTN: TECHNICAL STAFF (PLS ROUTE)
PO BOX 999, MS K6-40
RICHLAND, WA 99352

PACIFIC NORTHWEST NATIONAL LABORATORY
ATTN: TECHNICAL STAFF (PLS ROUTE)
PO BOX 999, MS K5-12
RICHLAND, WA 99352

ANATOLI L. LEVSHIN
DEPARTMENT OF PHYSICS
UNIVERSITY OF COLORADO
CAMPUS BOX 390
BOULDER, CO 80309-0309

LOS ALAMOS NATIONAL LABORATORY
ATTN: TECHNICAL STAFF (PLS ROUTE)
PO BOX 1663, MS F659
LOS ALAMOS, NM 87545

LOS ALAMOS NATIONAL LABORATORY
ATTN: TECHNICAL STAFF (PLS ROUTE)
PO BOX 1663, MS D460
LOS ALAMOS, NM 87545

GARY MCCARTOR
SOUTHERN METHODIST UNIVERSITY
DEPARTMENT OF PHYSICS
DALLAS, TX 75275-0395

BRIAN MITCHELL
DEPARTMENT OF EARTH & ATMOSPHERIC SCIENCES
ST. LOUIS UNIVERSITY
3507 LACLEDE AVENUE
ST. LOUIS, MO 63103

JOHN MURPHY
MAXWELL TECHNOLOGIES
11800 SUNRISE VALLEY DRIVE SUITE 1212
RESTON, VA 22091

JOHN ORCUTT
INSTITUTE OF GEOPHYSICS AND PLANETARY PHYSICS
UNIVERSITY OF CALIFORNIA, SAN DIEGO
LA JOLLA, CA 92093

PACIFIC NORTHWEST NATIONAL LABORATORY
ATTN: TECHNICAL STAFF (PLS ROUTE)
PO BOX 999, MS K7-34
RICHLAND, WA 99352

PACIFIC NORTHWEST NATIONAL LABORATORY
ATTN: TECHNICAL STAFF (PLS ROUTE)
PO BOX 999, MS K6-84
RICHLAND, WA 99352

FRANK PILOTTE
HQ/AFTAC/TT
1030 S. HIGHWAY A1A
PATRICK AFB, FL 32925-3002

KEITH PRIESTLEY
DEPARTMENT OF EARTH SCIENCES
UNIVERSITY OF CAMBRIDGE
MADINGLEY RISE, MADINGLEY ROAD
CAMBRIDGE, CB3 OEZ UK

PAUL RICHARDS
COLUMBIA UNIVERSITY
LAMONT-DOHERTY EARTH OBSERVATORY
PALISADES, NY 10964

CHANDAN SAIKIA
WOOODWARD-CLYDE FEDERAL SERVICES
566 EL DORADO ST., SUITE 100
PASADENA, CA 91101-2560

SANDIA NATIONAL LABORATORY
ATTN: TECHNICAL STAFF (PLS ROUTE)
DEPT. 5791
MS 0567, PO BOX 5800
ALBUQUERQUE, NM 87185-0567

SANDIA NATIONAL LABORATORY
ATTN: TECHNICAL STAFF (PLS ROUTE)
DEPT. 5704
MS 0655, PO BOX 5800
ALBUQUERQUE, NM 87185-0655

THOMAS SERENO JR.
SCIENCE APPLICATIONS INTERNATIONAL
CORPORATION
10260 CAMPUS POINT DRIVE
SAN DIEGO, CA 92121

ROBERT SHUMWAY
410 MRAK HALL
DIVISION OF STATISTICS
UNIVERSITY OF CALIFORNIA
DAVIS, CA 95616-8671

DAVID SIMPSON
IRIS
1200 NEW YORK AVE., NW
SUITE 800
WASHINGTON, DC 20005

BRIAN SULLIVAN
BOSTON COLLEGE
INSITUTE FOR SPACE RESEARCH
140 COMMONWEALTH AVENUE
CHESTNUT HILL, MA 02167

NAFI TOKSOZ
EARTH RESOURCES LABORATORY, M.I.T.
42 CARLTON STREET, E34-440
CAMBRIDGE, MA 02142

JAY PULLI
BBN
1300 NORTH 17TH STREET
ROSSLYN, VA 22209

DAVID RUSSELL
HQ AFTAC/TTR
1030 SOUTH HIGHWAY A1A
PATRICK AFB, FL 32925-3002

SANDIA NATIONAL LABORATORY
ATTN: TECHNICAL STAFF (PLS ROUTE)
DEPT. 5704
MS 0979, PO BOX 5800
ALBUQUERQUE, NM 87185-0979

SANDIA NATIONAL LABORATORY
ATTN: TECHNICAL STAFF (PLS ROUTE)
DEPT. 9311
MS 1159, PO BOX 5800
ALBUQUERQUE, NM 87185-1159

SANDIA NATIONAL LABORATORY
ATTN: TECHNICAL STAFF (PLS ROUTE)
DEPT. 5736
MS 0655, PO BOX 5800
ALBUQUERQUE, NM 87185-0655

AVI SHAPIRA
SEISMOLOGY DIVISION
THE INSTITUTE FOR PETROLEUM RESEARCH AND
GEOPHYSICS
P.O.B. 2286, NOLON 58122 ISRAEL

MATTHEW SIBOL
ENSCO, INC.
445 PINEDA COURT
MELBOURNE, FL 32940

JEFFRY STEVENS
MAXWELL TECHNOLOGIES
8888 BALBOA AVE.
SAN DIEGO, CA 92123-1506

DAVID THOMAS
ISEE
29100 AURORA ROAD
CLEVELAND, OH 44139

LAWRENCE TURNBULL
ACIS
DCI/ACIS
WASHINGTON, DC 20505

GREG VAN DER VINK
IRIS
1200 NEW YORK AVE., NW
SUITE 800
WASHINGTON, DC 20005

TERRY WALLACE
UNIVERSITY OF ARIZONA
DEPARTMENT OF GEOSCIENCES
BUILDING #77
TUCSON, AZ 85721

JAMES WHITCOMB
NSF
NSF/ISC OPERATIONS/EAR-785
4201 WILSON BLVD., ROOM785
ARLINGTON, VA 22230

JIAKANG XIE
COLUMBIA UNIVERSITY
LAMONT DOHERTY EARTH OBSERVATORY
ROUTE 9W
PALISADES, NY 10964

OFFICE OF THE SECRETARY OF DEFENSE
DDR&E
WASHINGTON, DC 20330

TACTEC
BATTELLE MEMORIAL INSTITUTE
505 KING AVENUE
COLUMBUS, OH 43201 (FINAL REPORT)

PHILLIPS LABORATORY
ATTN: GPE
29 RANDOLPH ROAD
HANSCOM AFB, MA 01731-3010

PHILLIPS LABORATORY
ATTN: PL/SUL
3550 ABERDEEN AVE SE
KIRTLAND, NM 87117-5776 (2 COPIES)

FRANK VERNON
UNIVERSITY OF CALIFORNIA, SAN DIEGO
SCRIPPS INSTITUTION OF OCEANOGRAPHY IGPP, 0225
9500 GILMAN DRIVE
LA JOLLA, CA 92093-0225

DANIEL WEILL
NSF
EAR-785
4201 WILSON BLVD., ROOM 785
ARLINGTON, VA 22230

RU SHAN WU
UNIVERSITY OF CALIFORNIA SANTA CRUZ
EARTH SCIENCES DEPT.
1156 HIGH STREET
SANTA CRUZ, CA 95064

JAMES E. ZOLLWEG
BOISE STATE UNIVERSITY
GEOSCIENCES DEPT.
1910 UNIVERSITY DRIVE
BOISE, ID 83725

DEFENSE TECHNICAL INFORMATION CENTER
8725 JOHN J. KINGMAN ROAD
FT BELVOIR, VA 22060-6218 (2 COPIES)

PHILLIPS LABORATORY
ATTN: GPBP
29 RANDOLPH ROAD
HANSCOM AFB, MA 01731-3010

PHILLIPS LABORATORY
ATTN: RESEARCH LIBRARY/TL
5 WRIGHT STREET
HANSCOM AFB, MA 01731-3004